Article

SOURCE DATA | TRANSPARENT PROCESS

THE EMBO JOURNAL

PARL partitions the lipid transfer protein STARD7 between the cytosol and mitochondria

Shotaro Saita[1,†], Takashi Tatsuta[1], Philipp A Lampe[1], Tim König[1,‡], Yohsuke Ohba[1] & Thomas Langer[1,2,3,*]

Abstract

Intramembrane-cleaving peptidases of the rhomboid family regulate diverse cellular processes that are critical for development and cell survival. The function of the rhomboid protease PARL in the mitochondrial inner membrane has been linked to mitophagy and apoptosis, but other regulatory functions are likely to exist. Here, we identify the START domain-containing protein STARD7 as an intramitochondrial lipid transfer protein for phosphatidylcholine. We demonstrate that PARL-mediated cleavage during mitochondrial import partitions STARD7 to the cytosol and the mitochondrial intermembrane space. Negatively charged amino acids in STARD7 serve as a sorting signal allowing mitochondrial release of mature STARD7 upon cleavage by PARL. On the other hand, membrane insertion of STARD7 mediated by the TIM23 complex promotes mitochondrial localization of mature STARD7. Mitochondrial STARD7 is necessary and sufficient for the accumulation of phosphatidylcholine in the inner membrane and for the maintenance of respiration and cristae morphogenesis. Thus, PARL preserves mitochondrial membrane homeostasis via STARD7 processing and is emerging as a critical regulator of protein localization between mitochondria and the cytosol.

Keywords lipid transfer protein; mitochondria; PARL; rhomboid; STARD7
Subject Categories Membrane & Intracellular Transport
DOI 10.15252/embj.201797909 | Received 1 August 2017 | Revised 12 December 2017 | Accepted 13 December 2017 | Published online 4 January 2018
The EMBO Journal (2018) 37: e97909

See also: **T Endo & Y Tamura** (February 2017)

Introduction

Proteases residing within mitochondria perform essential roles in mitochondrial homeostasis (Quiros *et al*, 2015). They act as quality control enzymes degrading damaged polypeptides and control the processing or stability of regulatory proteins involved in diverse mitochondrial activities, from mitochondrial gene expression, protein, and lipid biogenesis to mitochondrial dynamics. The inner membrane protease PARL (presenilin-associated rhomboid-like) belongs to the evolutionary conserved family of intramembrane-cleaving rhomboid proteases, which cleave their substrates typically within transmembrane segments and release membrane-exposed domains (Urban, 2016; Dusterhoft *et al*, 2017). The loss of PARL or its homologues has profound effects on cell viability in diverse organisms (Spinazzi & De Strooper, 2016). PARL-deficient mice die before the age of 3 month due to muscle atrophy and excessive cell death in spleen and thymus (Cipolat *et al*, 2006). Moreover, PARL expression is decreased in skeletal muscle of patients with type 2 diabetes mellitus (Civitarese *et al*, 2010).

The first identified substrate of PARL was the mitochondrial kinase PINK1, which regulates mitophagy (Jin *et al*, 2010), the formation of mitochondria-derived vesicles (McLelland *et al*, 2014), and the activity of respiratory complex I (Morais *et al*, 2014). PINK1 cleavage within its transmembrane domain by PARL allows the release of mature PINK1 from mitochondria and results in its degradation by the ubiquitin–proteasome system (Yamano & Youle, 2013). In depolarized mitochondria, however, PINK1 insertion into the IM is impaired preventing cleavage by PARL. PINK1 accumulates at the mitochondrial surface under these conditions, where it induces mitophagy in concert with the ubiquitin ligase Parkin (Narendra *et al*, 2010; Whitworth & Pallanck, 2017). In contrast to PINK1, PARL-mediated processing of another substrate protein, the mitochondrial phosphatase PGAM5, is stimulated in dysfunctional mitochondria (Sekine *et al*, 2012). PGAM5 has been functionally linked to the regulation of mitochondrial dynamics, mitophagy, and cell death. It dephosphorylates various proteins localized at the outer membrane (OM) or in the cytosol (Takeda *et al*, 2009; Wang *et al*, 2012; Chen *et al*, 2014; Panda *et al*, 2016; Rauschenberger *et al*, 2017), suggesting that cleaved PGAM5 can be released from mitochondria. We recently identified in a proteomic survey the pro-apoptotic protein Smac (DIABLO), the complex III surveillance factor TTC19 (Ghezzi *et al*, 2011; Bottani *et al*, 2017), the lipid transfer protein (LTP) STARD7 (Horibata & Sugimoto, 2010), and CLPB (Capo-Chichi *et al*, 2015; Kanabus *et al*, 2015; Saunders *et al*, 2015; Wortmann *et al*, 2015) as additional

1 Institute for Genetics and Cologne Excellence Cluster on Cellular Stress Responses in Aging-Associated Diseases (CECAD), University of Cologne, Cologne, Germany
2 Center for Molecular Medicine (CMMC), University of Cologne, Cologne, Germany
3 Max-Planck-Institute for Biology of Ageing, Cologne, Germany
*Corresponding author. Tel: +49 221 478 84263; Fax: +49 221 478 84261; E-mail: thomas.langer@uni-koeln.de; langer@age.mpg.de
†Present address: Department of Genetics, Graduate School of Medicine, Osaka University, Osaka, Japan
‡Present address: Department of Neurology and Neurosurgery, Montreal Neurological Institute, McGill University, Montreal, QC, Canada

substrates of PARL, highlighting the pleiotropic roles of PARL in mitochondria and its relevance for disease (Saita *et al*, 2017). In apoptotic cells, PARL-mediated cleavage of Smac is required for the BAX/BAK-dependent release of Smac from mitochondria into the cytosol, where Smac binds the inhibitor of apoptosis XIAP and allows apoptosis to proceed (Saita *et al*, 2017).

STARD7 is a member of the START (StAR-related lipid transfer) domain-containing family of LTPs (Alpy & Tomasetto, 2014) and was shown to specifically transfer phosphatidylcholine (PC) between liposomes *in vitro* (Horibata & Sugimoto, 2010; Horibata *et al*, 2016). Mutations in *STARD7* have been associated with acute asthma, and heterozygous *Stard7*$^{+/-}$ mice show increased permeability of the lung epithelium (Yang *et al*, 2015, 2017). The loss of STARD7 in mouse hepatoma cells impairs the accumulation of PC in mitochondrial membranes as well as mitochondrial ATP production and cristae morphogenesis (Horibata *et al*, 2016). STARD7 has been localized at the mitochondrial OM and in the cytosol and was suggested to mediate PC transfer from the cytosol to mitochondrial membranes (Horibata & Sugimoto, 2010; Horibata *et al*, 2017). However, it remains unclear how this function can be reconciled with PARL-mediated maturation of STARD7 at the IM (Saita *et al*, 2017).

Here, we demonstrate that STARD7 localizes both to the cytosol and the mitochondrial intermembrane space (IMS), where it serves as an intramitochondrial LTP for PC. Our experiments reveal that PARL and specific sorting signals in STARD7 modulate the partitioning of newly imported STARD7 between two different mitochondrial import pathways and ensure the dual localization of STARD7. PARL is thus emerging as a critical regulator of protein localization and of communication pathways between mitochondria and the cytosol.

Results

PARL regulates the dual localization of STARD7 to mitochondria and the cytosol

The identification of STARD7 as a substrate of PARL suggests that STARD7 is imported into mitochondria after its synthesis on cytosolic ribosomes. We therefore performed cellular fractionation experiments to monitor the subcellular distribution of STARD7 in human cells. In agreement with previous reports (Horibata & Sugimoto, 2010; Horibata *et al*, 2016), STARD7 was detected in the cytosol (Fig 1A). However, almost 60% of the protein was recovered from the mitochondrial fraction, while about 20% were found in association with microsomes (Fig 1A). Further purification of mitochondria by density gradient centrifugation confirmed the dual localization of STARD7 to mitochondria and the cytosol (Fig EV1A).

These results were substantiated using immunofluorescence microscopy of *PARL*$^{+/+}$ and *PARL*$^{-/-}$ HeLa cells expressing STARD7 (Figs 1B–D and EV1B). STARD7 was detected in the cytosol but also co-localized with mitochondrial TOMM20 in *PARL*$^{+/+}$ cells (Fig 1B–D). Strikingly, STARD7 was quantitatively retained in mitochondria upon expression in *PARL*$^{-/-}$ cells (Fig 1B–D). Thus, PARL is required for the cytosolic localization of STARD7 indicating that newly synthesized STARD7 is first imported into mitochondria before redistribution to the cytosol occurs.

To further corroborate the critical role of PARL for the dual localization of STARD7, we replaced the amino terminal region of STARD7 by an unrelated mitochondrial targeting sequence, which is cleaved off by another mitochondrial protease. We chose the amino terminal amino region of mitochondrial calcium uptake 1 (MICU1; Perocchi *et al*, 2010), which is sorted to the IMS by a mitochondrial targeting sequence and a transmembrane segment and which is converted into the mature form by the IMMP1L protease in the IMS (Fig EV1C). STARD7 or a chimeric protein consisting of the mitochondrial targeting sequence of MICU1 (amino acids 1–60) and mature STARD7 (amino acids 77–370) (MICU1-STARD7) were stably expressed in *STARD7*$^{-/-}$ cells (Fig 1E and F), which were generated by CRISPR/Cas9-mediated genome editing. MICU1-STARD7 was targeted to mitochondria and converted into its mature form (Fig 1F). Immunofluorescence studies confirmed the mitochondrial localization of MICU1-STARD7 (Fig 1G and H). In contrast to STARD7-expressing cells, we did not detect the accumulation of mature STARD7 in the cytosolic fraction of *STARD7*$^{-/-}$ cells expressing MICU1-STARD7 (Fig 1F–H). Thus, maturation of STARD7 by IMMP1L precludes the cytosolic localization of STARD7, which is observed upon processing by PARL. We therefore conclude that cleavage by PARL is required for mitochondrial release and the dual localization of STARD7 to mitochondria and the cytosol.

Sorting of STARD7 to the IMS involves two-step processing

To define how PARL affects sorting of STARD7, we first determined the localization of STARD7 within mitochondria and fractionated

Figure 1. PARL regulates dual localization of STARD7.

A Fractionation of HeLa cells into post nuclear (PNS), mitochondrial (Mito), microsomal (Micro), and cytosolic (Cyto) fractions. Left panel: samples were analyzed by SDS–PAGE and immunoblotting. Right panel; quantification of intensities (n = 3; mean values ± SD).

B Immunofluorescence analysis of wild-type (WT) and *PARL*$^{-/-}$ HeLa cells. HeLa cells stably expressing FLAG-tagged human STARD7 were examined by immunofluorescence staining using FLAG- (*green*) and TOMM20- (*red*) specific antibodies. Nuclei were stained with DAPI (*blue*). Scale bars, 10 μm. Parts shown in higher magnification are boxed; scale bars, 10 μm. Lines are scanned in (C).

C Line scans of arrows indicated in (B).

D Quantification of (C) (n = 3; mean values ± SD; number of cells ≥ 70).

E Domain organization of STARD7 and MICU1-STARD7. The chimeric protein consists of amino acids 1–60 of MICU1 (including the IMMP1L processing site) and amino acids 77–370 of STARD7. MTS, mitochondrial target sequence. TM, transmembrane domain. START, StAR-related lipid transfer domain.

F Fractionation of *STARD7*$^{-/-}$ HeLa cells complemented with STARD7^{FLAG} or MICU1-STARD7^{FLAG} cells into mitochondrial (Mito) and cytosolic (Cyto) fractions. Samples were analyzed by SDS–PAGE and immunoblotting using STARD7-specific antibodies.

G Immunofluorescence analysis of *STARD7*$^{-/-}$ HeLa cells complemented with MICU1-STARD7^{FLAG}. Cells were stained with FLAG- (*green*) and TOMM20- (*red*) specific antibodies. Nuclei were stained with DAPI (*blue*). Scale bars, 10 μm. Line is scanned in (H).

H Line scan of arrow indicated in (G).

Source data are available online for this figure.

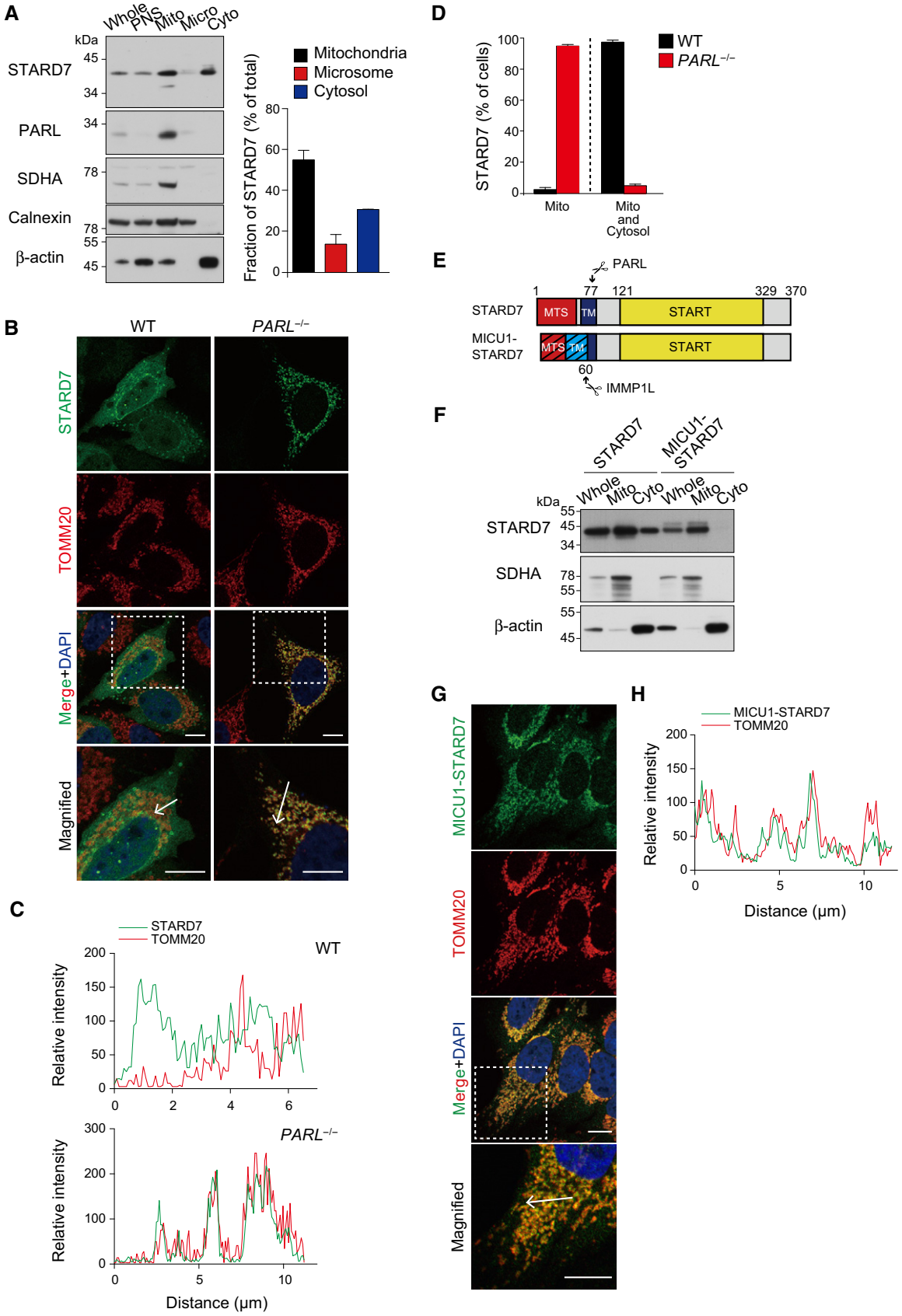
A
Whole
PNS
Mito
Micro
Cyto
kDa
STARD7
PARL
SDHA
Calnexin
β-actin
Mitochondria
Microsome
Cytosol
Fraction of STARD7 (% of total)
B
WT
PARL−/−
STARD7
TOMM20
Merge+DAPI
Magnified
C
STARD7
TOMM20
WT
PARL−/−
Relative intensity
Distance (μm)
D
STARD7 (% of cells)
WT
PARL−/−
Mito
Mito and Cytosol
E
PARL
STARD7
MICU1-STARD7
MTS
TM
START
IMMP1L
F
STARD7
MICU1-STARD7
G
MICU1-STARD7
TOMM20
Merge+DAPI
Magnified
H
MICU1-STARD7
TOMM20
Relative intensity
Distance (μm)

Figure 1.

mitochondria purified from *PARL*$^{+/+}$ cells by osmotic swelling (Fig 2A). In contrast to previous reports (Horibata *et al*, 2017), STARD7 was protected against externally added protease in intact mitochondria but was degraded upon disruption of the OM (Fig 2A). It thus shows a similar behavior than the *i*-AAA protease YME1L, which is active in the IMS, whereas matrix-localized proteins such as mtHSP70 became accessible to externally added protease only upon solubilization of the IM (Fig 2A). STARD7 was recovered in the supernatant fraction upon alkaline extraction of mitochondrial membranes, indicating that it is not inserted into mitochondrial membranes (Fig EV2A).

While inhibiting the accumulation of STARD7 in the cytosol, the loss of PARL in *PARL*$^{-/-}$ cells did not affect its localization to the IMS (Fig 2A). We observed the accumulation of larger forms of STARD7 in the mitochondrial IMS (Fig 2A). STARD7 maturation was only partially impaired in *PARL*$^{-/-}$ cells, suggesting that other mitochondrial protease(s) can substitute for the function of PARL. To unambiguously demonstrate PARL-mediated cleavage of STARD7, PARL or PARL^{S277A} harboring a point mutation in the catalytic center was synthesized in a cell-free system and reconstituted in liposomes (Fig 2B), which were then incubated with recombinant STARD7. STARD7 was converted into its mature form by PARL but not by PARL^{S277A} demonstrating that PARL cleaves STARD7 (Fig 2C and D). Consistently, expression of PARL but not of PARL^{S277A} restored maturation of STARD7 in *PARL*$^{-/-}$ cells (Fig EV2B).

Our previous proteomic analysis identified Ala78 as the N-terminal amino acid residue of mature STARD7 (Saita *et al*, 2017). PARL thus cleaves STARD7 within the putative transmembrane domain between amino acid residues 68 and 86 (Fig EV2C). Consistently, larger forms of STARD7 were mainly recovered in the pellet fraction upon alkaline extraction of mitochondrial membranes, indicating that they are more tightly associated with these membranes (Fig EV2A).

The accumulation of intermediate-sized forms of STARD7 in *PARL*$^{-/-}$ cells suggests two-step processing of STARD7 and the involvement of another peptidase. STARD7 contains a predicted mitochondrial targeting sequence containing a consensus cleavage site for the matrix-localized mitochondrial processing peptidase MPP after amino acid 65. Downregulation of MPP in *PARL*$^{-/-}$ cells impaired the formation of the intermediate forms and resulted in the accumulation of the precursor form of STARD7 (Fig EV2D). We conclude that two peptidases, MPP and PARL, convert newly imported STARD7 into its mature form, which is localized in the IMS (Fig EV2E).

Notably, STARD7 was degraded when cells were incubated in the presence of cycloheximide to inhibit protein synthesis (Fig 2E and F). However, STARD7 accumulated stably in cells lacking the *i*-AAA protease YME1L, indicating that degradation is mediated by the *i*-AAA protease YME1L (Fig 2E and F). These results corroborate the localization of STARD7 to the mitochondrial IMS.

PARL cleavage allows mitochondrial release of newly imported STARD7

The requirement of PARL for the cytosolic localization of STARD7 indicates redistribution of STARD7 from mitochondria to the cytosol. To monitor whether mitochondrial STARD7 can be released from the IMS, we incubated mitochondria and analyzed proteins accumulating in the supernatant after centrifugation (Fig EV3A). However, endogenous, mature STARD7 was not released from mitochondria (Fig EV3A), suggesting that STARD7 is released during import into mitochondria. We therefore assessed maturation and mitochondrial accumulation of STARD7 in protein import experiments *in vitro* (Fig 3A). STARD7 was synthesized in a cell-free system and incubated with isolated mitochondria. We observed maturation of STARD7 in a membrane potential-dependent manner (Fig 3A). Mature STARD7 but not its precursor form was protected against externally added protease (Fig 3B), demonstrating that mature STARD7 was imported into mitochondria.

To monitor the distribution of STARD7 between mitochondria and the cytosol, we performed protein import experiments using mitochondria isolated from *PARL*$^{+/+}$ and *PARL*$^{-/-}$ cells. Mitochondria were separated from supernatants at various times after initiation of the import reaction, and both fractions were analyzed for the presence of mature STARD7 (Fig 3C). As expected, we detected mature STARD7 not only in mitochondria but to similar amounts also in the supernatant fraction upon incubation of newly synthesized STARD7 with *PARL*$^{+/+}$ mitochondria (Fig 3C). Other mitochondrial proteins, such as Smac or SDHA, a subunit of the succinate dehydrogenase complex, were not present in this fraction excluding an unspecific release of IMS proteins or mitochondrial contamination of this fraction (Fig 3C). Maturation of newly imported STARD7 was inhibited in *PARL*$^{-/-}$ mitochondria and STARD7 did not accumulate in the supernatant fraction, demonstrating that release of STARD7 requires cleavage by PARL (Fig 3C). These results substantiate the requirement of PARL for the cytosolic localization of STARD7 (Fig 1).

We determined the fraction of newly imported STARD7 that is released from mitochondria at different time points during the import reaction (Fig 3D and E). Maturation of STARD7 proceeded over time,

Figure 2. PARL mediates maturation of STARD7.

A Fractionation of mitochondria isolated from HEK293 cells. Accessibility of mitochondrial proteins to externally added proteinase K (PK) was assessed upon osmotic swelling of mitochondria and after membrane solubilization with Triton X-100 (Triton). Fractions were analyzed by SDS–PAGE and immunoblotting using the following antibodies: TOMM20 (OM), YME1L (IM), PARL (IM), and mtHSP70 (matrix). p, precursor; i, intermediate; m, mature form of STARD7.

B Reconstitution of PARL into proteoliposomes and STARD7 processing.

C STARD7^{HA} synthesized in a reticulocyte cell-free system was incubated with proteoliposomes containing reconstituted PARL^{His} or PARL(S277A)^{His} for the indicated times. Samples were analyzed by SDS–PAGE and immunoblotting. p, precursor; m, mature form of STARD7. *, second translation product.

D Quantification of (C) (n = 3; each symbol represents data from one experiment). Mature STARD7^{HA} at 4 h was set to 100%.

E YME1L degrades STARD7 in the IMS. Wild-type (WT) or *YME1L*$^{-/-}$ HEK cells were incubated with cycloheximide (75 μg/ml) for the indicated times. Cell lysates were analyzed by SDS–PAGE, and fluorescence intensities were detected using the infrared Odyssey system for STARD7 and SDHA.

F Quantification of (E) (n = 3; mean values ± SD). ****$P < 0.0001$, one-way ANOVA.

Source data are available online for this figure.

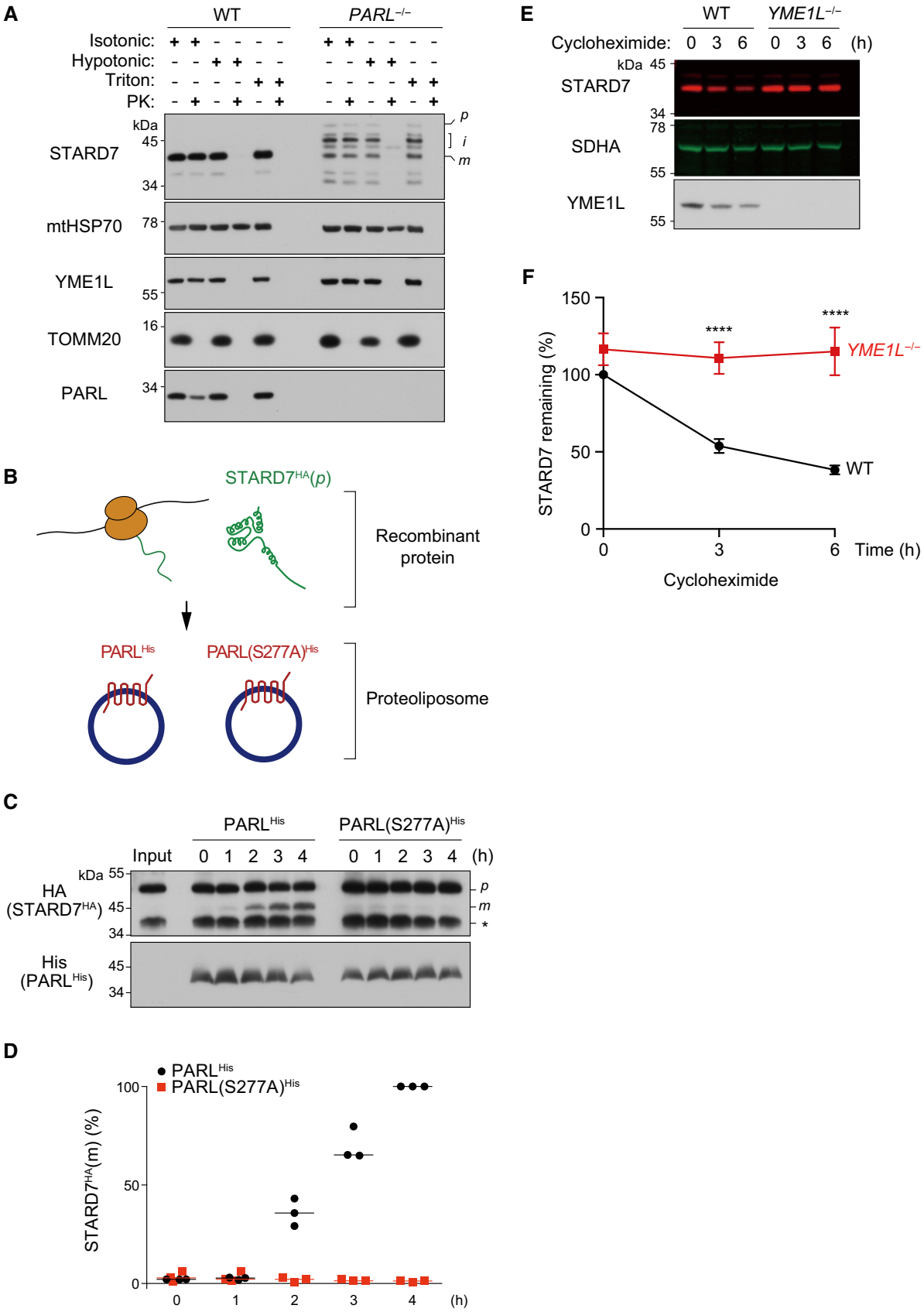
A
WT
PARL−/−
Isotonic:
Hypotonic:
Triton:
PK:
kDa
STARD7
mtHSP70
YME1L
TOMM20
PARL
p
i
m
B
STARD7HA(p)
Recombinant protein
PARLHis
PARL(S277A)His
Proteoliposome
C
PARLHis
PARL(S277A)His
Input
(h)
HA (STARD7HA)
His (PARLHis)
D
PARLHis
PARL(S277A)His
STARD7HA(m) (%)
E
WT
YME1L−/−
Cycloheximide:
SDHA
F
STARD7 remaining (%)
YME1L−/−
WT
Time (h)
Cycloheximide
****

Figure 2.

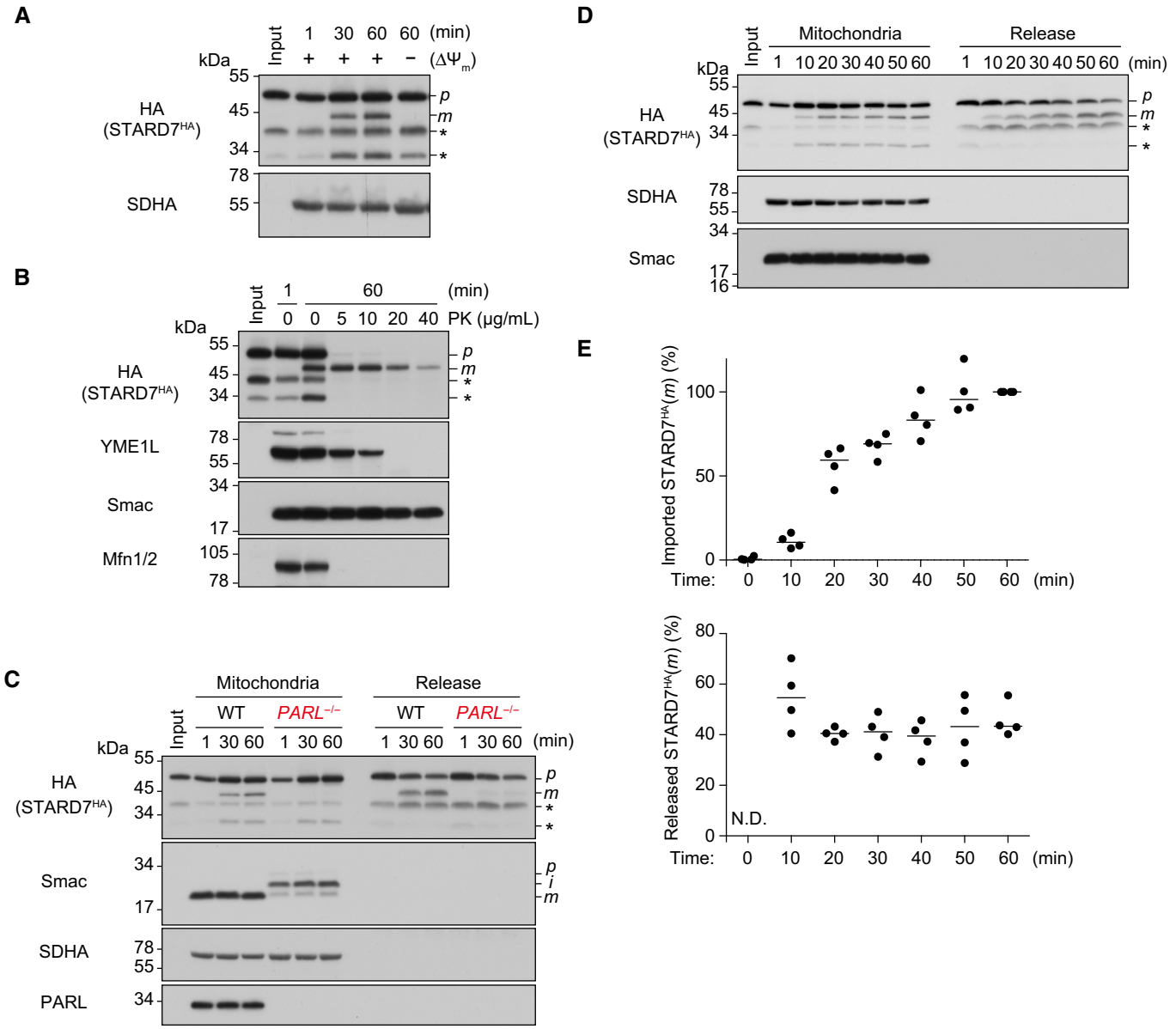

Figure 3. PARL-mediated cleavage during import allows release of STARD7 from mitochondria.

A Import and maturation of STARD7 in mitochondria. STARD7^{HA} was synthesized in a cell-free system and incubated in the presence or absence of CCCP (2 mM) with mitochondria that were isolated from HEK293 cells. Import was halted at the indicated time points, and samples were analyzed by SDS–PAGE and immunoblotting. Input (20%); p, precursor; m, mature form. *, second translation products.

B Mature STARD7 is localized in the IMS. STARD7^{HA} was imported into HEK293 mitochondria. Samples were treated with proteinase K (PK) for 15 min at 4°C as indicated and analyzed by SDS–PAGE and immunoblotting. Input (20%); p, precursor; m, mature form. *, second translation products.

C PARL-dependent release of mature STARD7 from mitochondria. STARD7^{HA} was incubated with mitochondria isolated from either wild-type (WT) or *PARL*$^{-/-}$ HEK293 cells. Samples were split by centrifugation into pellet (Mitochondria) and supernatant (Release) fractions and analyzed by SDS–PAGE and immunoblotting. Input (20%); p, precursor; i, intermediate; m, mature form. *, second translation products.

D Kinetics of STARD7 maturation and release. STARD7^{HA} was imported for indicated times into mitochondria isolated from HEK293 cells as in (C). p, precursor; m, mature form. *, second translation products.

E Quantification of (D) (n = 4; each symbol represents data from one experiment). Mature STARD7^{HA} after 60 min of import was set to 100%. Released mature STARD7^{HA} is given as percentage of total mature STARD7^{HA}.

Source data are available online for this figure.

and ~40% of cleaved STARD7 was released from mitochondria at any given time point (Fig 3E), whereas endogenous STARD7 was not released (Fig EV3A). We conclude from these experiments that, while STARD7 cannot be released from mitochondria upon completion of import, PARL-mediated processing of STARD7 during import allows its partitioning between mitochondria and the cytosol.

Negatively charged amino acids promote the release of STARD7 from mitochondria

Other PARL substrate proteins, such as Smac or CLPB, were not released from mitochondria during *in vitro* import reactions (Fig EV3B and C), suggesting that additional signals determine protein localization after cleavage by PARL. We noted that a series of negatively charged amino acid residues are present after the PARL cleavage site in STARD7 but not in Smac or CLPB (Fig EV4A). To examine whether these amino acid residues impact on the distribution of STARD7 between mitochondria and the cytosol, we first deleted regions in STARD7 harboring the negatively charged amino acids (Fig 4A) and assessed the release of the resulting STARD7 variants during mitochondrial import (Fig 4B). Deletion of amino acid residues 86–120 of STARD7 abolished the release of mature STARD7 from mitochondria (Fig 4B). Similarly, STARD7 lacking amino acid residues 86–102 accumulated quantitatively in mitochondria, whereas a variant lacking amino acids 102–120 distributed between mitochondrial and supernatant fraction (Fig 4B). These experiments demonstrate that the efficient release of STARD7 from mitochondria depends on amino acids 86–102.

To further delineate the signal triggering mitochondrial release of STARD7, we replaced negatively charged amino acids in this region by alanine residues (Fig 4A; $STARD7^{AAA\text{-}1}$; $STARD7^{AAA\text{-}2}$; $STARD7^{AAA\text{-}3}$). Whereas $STARD7^{AAA\text{-}1}$ was cleaved by PARL with similar efficiency as STARD7, its release from mitochondria was significantly impaired (Fig 4C), demonstrating that aspartate and glutamate residues D86, E87, and E88 are required for partitioning of STARD7 to the cytosol. The removal of additional negatively charged amino acids in AAA-3 impaired both processing and mitochondrial release of STARD7 (Fig 4C).

To unambiguously demonstrate the crucial function of negatively charged amino acids for the dual localization of STARD7, we introduced amino acid residues 86–102 of STARD7 into the corresponding region of Smac ($Smac^{STARD7}$; Fig 4D), which is not released from mitochondria in non-apoptotic cells (Figs 3C and EV3B; Saita *et al*, 2017). Moreover, we replaced negatively charged amino acids within this region by alanine ($Smac^{STARD7\text{-}A}$; Fig 4D). Smac, $Smac^{STARD7}$, and $Smac^{STARD7\text{-}A}$ were imported into mitochondria, and the release of mature forms of these proteins was monitored (Fig 4E). In contrast to Smac, ~30% of mature $Smac^{STARD7}$ accumulated in the supernatant fraction demonstrating that the inserted amino acid sequence derived from STARD7 allows mitochondrial release. $Smac^{STARD7\text{-}A}$ remained associated with mitochondria (Figs 4E and EV4B), highlighting the crucial function of negatively charged amino acids in this region for the distribution of PARL substrate proteins between mitochondria and the cytosol.

TIMM23 promotes localization of STARD7 to mitochondria

PARL mediates the maturation of STARD7 cleaving the precursor form within its transmembrane domain (Fig EV2E). Newly imported mitochondrial proteins harboring one transmembrane domain are sorted to the IM by the TIM23 complex, a multisubunit protein translocase containing TIMM23 as a core component (Wiedemann & Pfanner, 2017). To examine how the TIM23 complex affects sorting and release of newly imported STARD7, we depleted TIMM23 from human cells, isolated mitochondria, and analyzed import and release of STARD7 (Fig 5A). In agreement with the TIM23 complex mediating membrane insertion of STARD7, mature STARD7 accumulated at reduced levels in mitochondria depleted of TIMM23 (Fig 5A and B). Surprisingly, the fraction of mature STARD7 that is released from mitochondria significantly increased upon depletion of TIMM23 (Fig 5C and D). These results suggest that retranslocation of mature STARD7 from mitochondria does not strictly depend on TIMM23, which rather appears to promote the localization of STARD7 to mitochondria. This interpretation is consistent with immunoprecipitation experiments in mitochondria harboring $PARL(S277A)^{FLAG}$ (Fig 5E and F). Depletion of TIMM23 did not affect binding of STARD7 to PARL during import indicating that TIMM23 is not essential for STARD7 processing by PARL. Thus, TIMM23 and internal signals in STARD7 determine the distribution of STARD7 between mitochondria and the cytosol.

Mitochondrial STARD7 preserves the structure and function of mitochondria

STARD7 has been described as a PC-specific LTP in the cytosol, which transports PC to the mitochondrial surface and thereby maintains the functional integrity of mitochondria (Horibata & Sugimoto,

Figure 4. Negatively charged amino acids in mature STARD7 are necessary and sufficient for mitochondrial release.

A Domain organization of human STARD7. The N-terminal amino acid sequence of mutant variants of mature STARD7 is shown. MTS, mitochondrial target sequence. TM, transmembrane domain. START, StAR-related lipid transfer domain.

B Maturation and mitochondrial release of STARD7 variants. $STARD7^{HA}$ mutants harboring deletions were incubated with HEK293 mitochondria for indicated times. Samples were split by centrifugation into pellet (Mitochondria) and supernatant (Release) fractions and analyzed by SDS–PAGE and immunoblotting. Cleaved and released fractions after 30-min import were quantified for different STARD7 variants (n = 3; each symbol represents data from one experiment). The red dotted line indicates the corresponding fraction of $STARD7^{HA}$ after 30-min import (from Fig 3E). Input (20%); p, precursor; m, mature form. #, second translation products. $^*P < 0.05$, $^{**}P < 0.01$, one-way ANOVA.

C Maturation and mitochondrial release of STARD7 mutants lacking negatively charged amino acids. $STARD7^{HA}$ variants harboring point mutations in negatively charged amino acid residues (see A) were incubated with HEK293 mitochondria for indicated times (as in B). Cleaved and released fractions after 30-min import were quantified for different STARD7 variants (n = 3; each symbol represents data from one experiment). The red dotted line indicates the corresponding fraction of $STARD7^{HA}$ after 30-min import (from Fig 3E). Input (20%); p, precursor; m, mature form. #, second translation products. $^*P < 0.05$, $^{**}P < 0.01$, one-way ANOVA.

D Amino acid sequence of the N-terminal region of mature Smac and variants thereof. The STARD7-derived peptide and its mutant derivative lacking negatively charged amino acids which are inserted into Smac in $Smac^{STARD7}$ and $Smac^{STARD7\text{-}A}$ are highlighted. Negatively and positively charged amino acids are shown in red or blue, respectively.

E Maturation and mitochondrial release of Smac and variants containing STARD7-derived peptides. Quantification of the released fraction of Smac and its variants at different time points of the import reaction is shown in the lower panel (n = 3; each symbol represents data from one experiment). The red dotted line indicates the released fraction of Smac, $Smac^{STARD7}$, and $Smac^{STARD7\text{-}A}$ (from Fig 3E). Input (20%); p, precursor; m, mature form. #, second translation product. $^{**}P < 0.01$, one-way ANOVA.

Source data are available online for this figure.

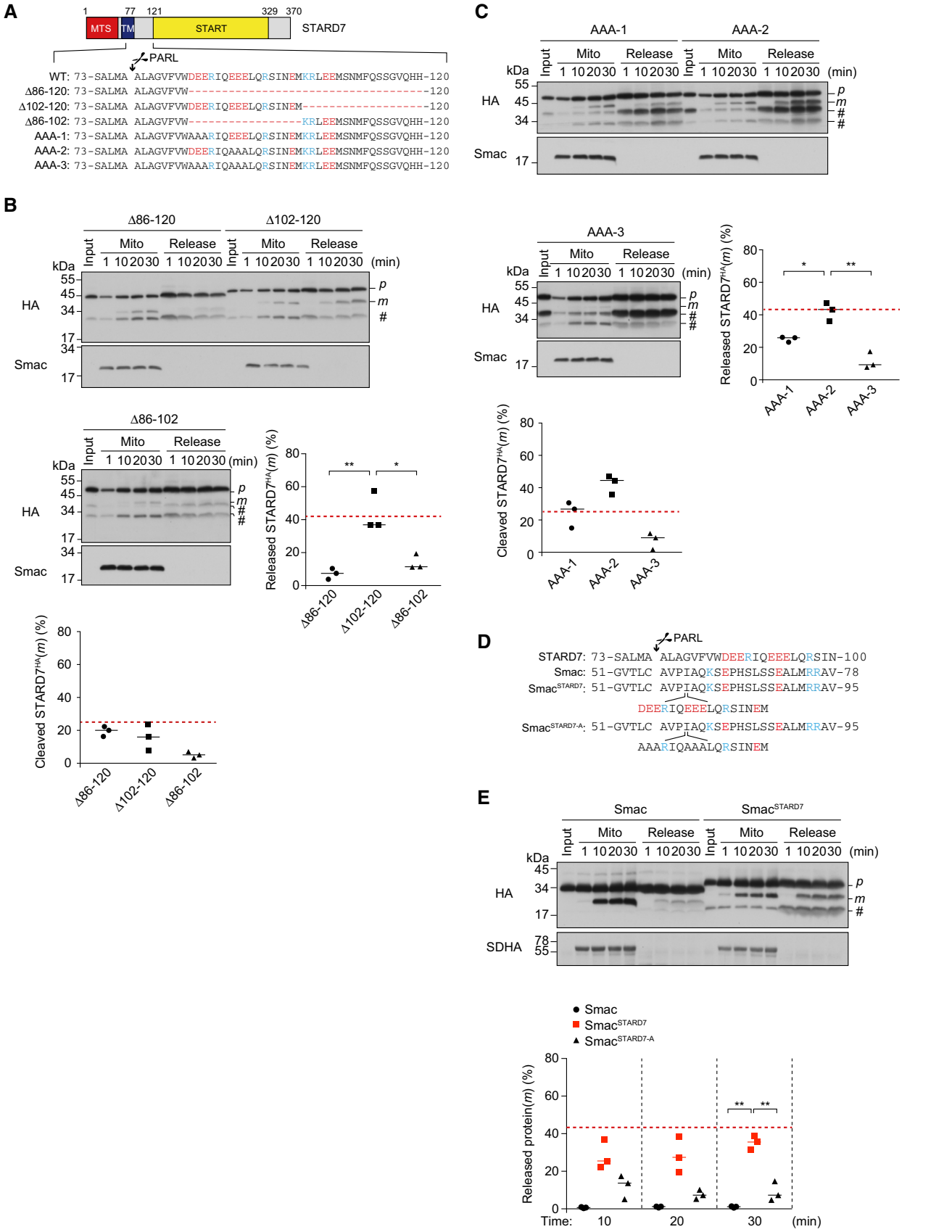

Figure 4.

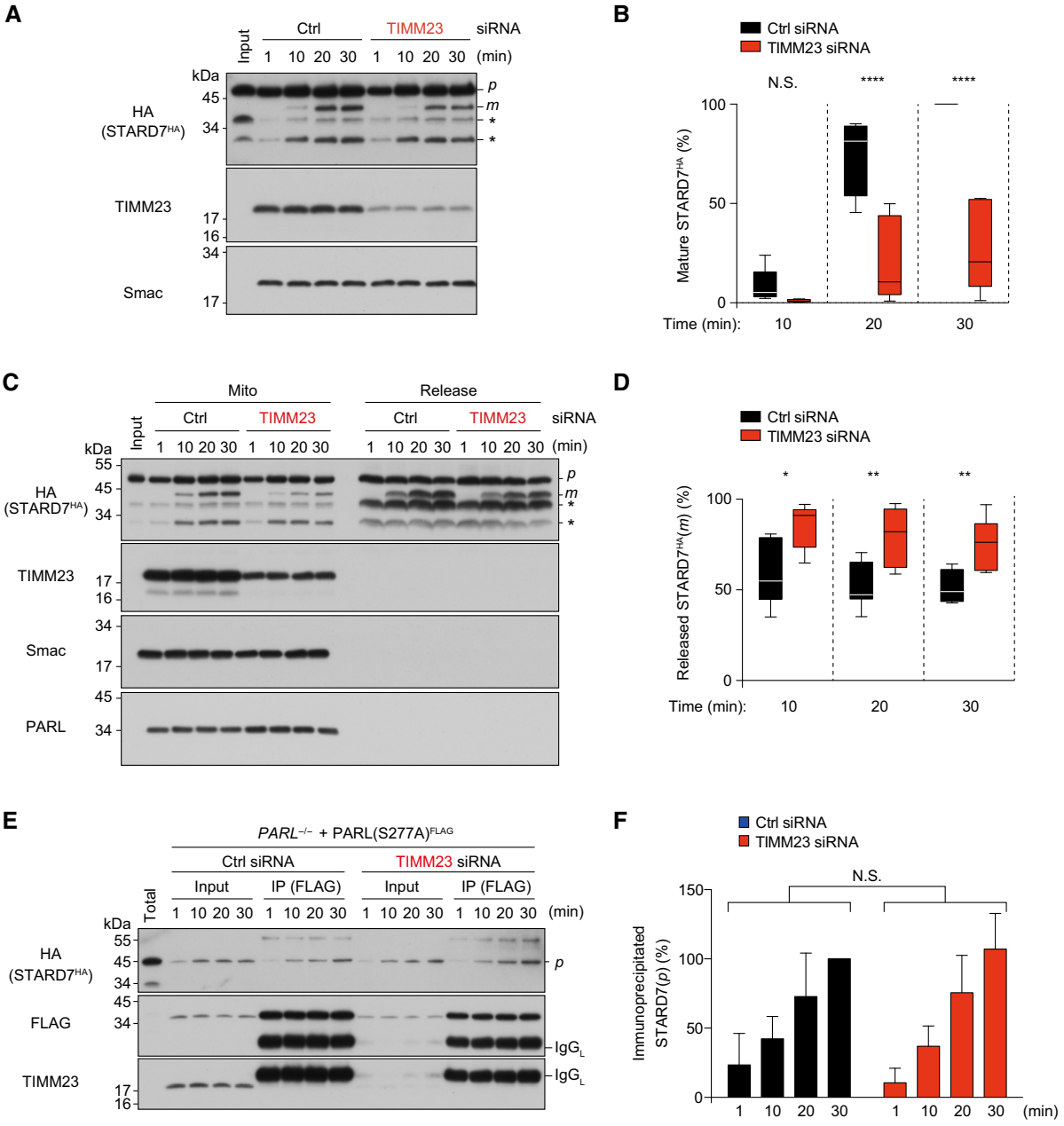

Figure 5. Depletion of TIMM23 facilitates the release of STARD7.

A TIMM23 depletion inhibits maturation of STARD7 in mitochondria. STARD7^{HA} was imported into mitochondria isolated from HEK293 cells that were siRNA-depleted of TIMM23 when indicated (as in Fig 3A). Input (20%); p, precursor; m, mature form. *, second translation products.

B Quantification of (A). Mature STARD7 released from control mitochondria after 30 min was set to 100% (n = 5). The box spans the first quartile to the third quartile, the horizontal line corresponds to the median and the whiskers above and below the box show the locations of the minimum and maximum values. ****$P < 0.0001$, one-way ANOVA.

C TIMM23 depletion facilitates release of mature STARD7. STARD7^{HA} was imported into mitochondria isolated from HEK293 cells that were siRNA-depleted of TIMM23 when indicated, and release of mature STARD7 was assessed as in Fig 3C. Input (20%); p, precursor; m, mature form. *, second translation products.

D Quantification of (C) (n = 7). The box spans the first quartile to the third quartile, the horizontal line corresponds to the median and the whiskers above and below the box show the locations of the minimum and maximum values. Mature STARD7 accumulating in mitochondria and the released fraction at each time point was set to 100%. *$P < 0.05$, **$P < 0.01$, one-way ANOVA.

E Depletion of TIMM23 does not impair PARL binding of STARD7. STARD7^{HA} was incubated for indicated times with mitochondria, which were isolated from *PARL*$^{-/-}$ HEK293 cells that express proteolytic inactive PARL(S277A)^{FLAG} and were depleted of TIMM23 by siRNA when indicated. Mitochondrial membranes were lysed with digitonin (5 g digitonin/g protein), and lysates were subjected to immunoprecipitation with FLAG-specific antibodies. Import reactions (10%) and immunoprecipitates (IP) were analyzed by SDS–PAGE and immunoblotting. Total, newly synthesized STARD7.

F Quantification of immunoprecipitated proteins of (E) is shown (n = 3; mean values ± SD). N.S., not significant, one-way ANOVA. p, precursor.

Source data are available online for this figure.

2010; Horibata *et al*, 2016). However, the localization of STARD7 within mitochondria raises the question whether mitochondrial deficiencies observed in *STARD7*$^{-/-}$ cells are caused by the loss of cytosolic or mitochondrial STARD7. We therefore expressed in *STARD7*$^{-/-}$ cells either the STARD7 precursor protein or mature STARD7 lacking the mitochondrial targeting sequence (STARD7-ΔN). Deletion of the N-terminal 76 amino acids of STARD7 did not affect its accumulation in the cytosol or its targeting to microsomes but impaired the accumulation of STARD7 in the mitochondrial fraction (Fig EV5A).

We observed severely impaired basal and maximum OCRs (Fig 6A–C), reduced cellular ATP levels (Fig 6D), and reduced levels of the cytochrome *c* oxidase subunit COXI in *STARD7*$^{-/-}$ cells (Fig 6E), as described previously (Horibata *et al*, 2016). These deficiencies were suppressed upon expression of STARD7 but not of STARD7-ΔN (Fig 6A–E), demonstrating that maintenance of mitochondrial activities depends on the import of STARD7 into mitochondria.

We next analyzed the morphology of mitochondria in *STARD7*$^{-/-}$ cells expressing STARD7 or STARD7-ΔN. Loss of STARD7 did not affect the formation of a tubular mitochondrial network. However, the formation of cristae was severely disturbed in *STARD7*$^{-/-}$ cells (Fig 6F and G; Horibata *et al*, 2016). Similar to mitochondrial respiratory functions, normal cristae morphogenesis required mitochondrial targeting of STARD7 and was only maintained in *STARD7*$^{-/-}$ cells upon expression of STARD7 but not of STARD7-ΔN (Fig 6F and G).

Several protein complexes in the IM maintain cristae morphogenesis including dimers of ATP synthase complexes (Paumard *et al*, 2002; Habersetzer *et al*, 2013), the dynamin-like GTPase OPA1 (Cipolat *et al*, 2006; Frezza *et al*, 2006), mitochondrial contact site and cristae organization system (MICOS) (Rampelt *et al*, 2017) as well as prohibitin complexes (Tatsuta & Langer, 2017). Whereas the loss of STARD7 did not affect the accumulation of OPA1 (Horibata *et al*, 2016), MICOS, and prohibitin complexes (Fig EV5B), we observed significantly reduced levels of dimers of ATP synthases upon Blue native-PAGE (BN-PAGE) analysis of STARD7-deficient mitochondrial extracts (Fig 6H). Dimerization of ATP synthases required mitochondrial STARD7 and was not restored upon expression of STARD7-ΔN (Fig 6H). Since dimers preserve mitochondrial cristae (Paumard *et al*, 2002; Habersetzer *et al*, 2013), the impaired dimerization of ATP synthases likely contributes to the disturbed cristae morphogenesis in cells lacking mitochondrial STARD7. These experiments establish critical functions of mitochondrial STARD7.

In contrast to this study, STARD7 has recently been reported to be localized to the mitochondrial OM (Horibata *et al*, 2017). To assess whether accumulation of STARD7 at the mitochondrial surface is sufficient to preserve mitochondrial activities, we replaced the mitochondrial targeting sequence and transmembrane region of STARD7 by the membrane anchor of the OM proteins TOMM70 or AKAP1 (Fig EV6A) and expressed these STARD7 variants in *STARD7*$^{-/-}$ cells. Both variants accumulated at mitochondria (Fig EV6B) but did not allow the accumulation of COX1 in these cells (Fig EV6C). Thus, neither cytosolic STARD7 nor STARD7 present at the mitochondrial surface is sufficient to preserve mitochondrial function.

To examine whether mitochondrial activities are preserved if STARD7 is only present in mitochondria, we analyzed *STARD7*$^{-/-}$ cells expressing MICU1-STARD7, which accumulate mature STARD7 in mitochondria but not in the cytosol (Fig 1F–H). Expression of STARD7 or MICU1-STARD7 restored efficient growth of *STARD7*$^{-/-}$ cells (Fig EV6D). Moreover, basal and maximal OCR, cellular ATP pools and the steady-state levels of COXI were restored in *STARD7*$^{-/-}$ cells harboring mitochondrial STARD7 only (Fig 6I–K). We therefore conclude that localization of STARD7 specifically to the IMS of mitochondria is necessary and sufficient to preserve mitochondrial functions.

STARD7 is an intramitochondrial lipid transfer protein for PC

We reasoned that STARD7 shuttles PC across the IMS and thereby maintains mitochondrial membrane homeostasis and function. To

Figure 6. Mitochondrial STARD7 is necessary and sufficient to preserve mitochondrial function.

Mitochondrial function was assessed in (A–H) wild-type (WT) and *STARD7*$^{-/-}$ HeLa cells and *STARD7*$^{-/-}$ HeLa cells complemented with STARD7 (WT) or mature STARD7 (amino acids 77–370; STARD7-ΔN) or in (I–K) WT and *STARD7*$^{-/-}$ HeLa cells and *STARD7*$^{-/-}$ HeLa cells complemented with MICU1-STARD7.

A Oxygen consumption rates (OCR) of cells cultured in glucose-containing medium (10 mM). Basal and maximal (2; 1.5 μM CCCP) OCR and the proton leak (1; 2 μM oligomycin A) are shown. Rotenone (0.5 μM) and antimycin A (0.5 μM) were used to block electron flow through complexes I and III (3). Mean ± SD of four replicates is shown. OCR was normalized to the amount of protein in the sample.

B Basal OCR of (A). ****$P < 0.0001$, one-way ANOVA.

C Maximum OCR of (A). **$P < 0.01$, ***$P < 0.001$, one-way ANOVA.

D Cellular ATP contents. Cells were cultured in galactose-containing medium (10 mM) overnight and further cultivated for 4 h in the presence or absence of 50 nM oligomycin A. The cellular ATP content was measured using the CellTiter-Glo Luminescent Cell Viability/ATP Assay kit ($n = 5$; mean values ± SD). ****$P < 0.0001$, one-way ANOVA.

E COXI protein levels. SDS–PAGE and immunoblot analyses of isolated mitochondria are shown in the left panel, a quantification of COXI protein levels in the right panel ($n = 3$; mean values ± SD). ***$P < 0.001$, N.S., not significant, one-way ANOVA.

F Transmission electron microscopy. Scale bars, 0.5 μm.

G Quantification of (F) (number of mitochondria analyzed: WT cells, 166; *STARD7*$^{-/-}$, 174, *STARD7*$^{-/-}$+WT, 176, *STARD7*$^{-/-}$+STARD7-ΔN, 139).

H BN-PAGE and SDS–PAGE analyses. Mitochondria were solubilized (1 g digitonin/g protein) and analyzed by BN-PAGE or SDS–PAGE, followed by immunoblotting with ATP5α-specific antibodies. V, monomer of ATP synthase; V_2, dimers of ATP synthases.

I Oxygen consumption rates (OCR) of cells cultured in glucose-containing medium (10 mM) (as in A). Mean ± SD of four replicates is shown. OCR was normalized to the amount of protein in the sample.

J Cellular ATP contents (as in D; $n = 5$ independent experiments; mean values ± SD). ****$P < 0.0001$, N.S., not significant, one-way ANOVA.

K COXI expression (as in E, left panel).

Source data are available online for this figure.

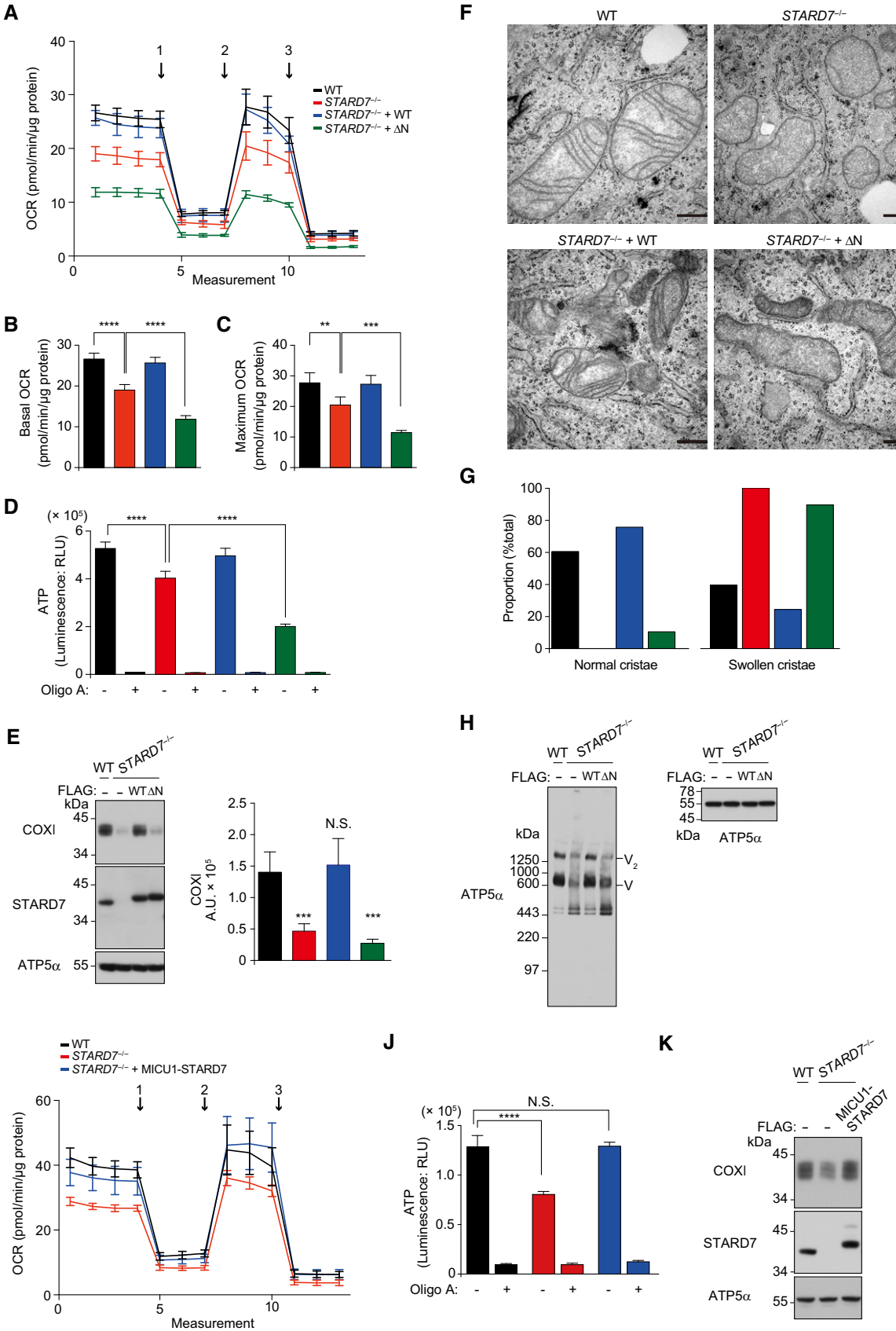
A
OCR (pmol/min/μg protein)
Measurement
WT
STARD7−/−
STARD7−/− + WT
STARD7−/− + ΔN
B
Basal OCR (pmol/min/μg protein)
C
Maximum OCR (pmol/min/μg protein)
D
ATP (Luminescence: RLU)
Oligo A:
E
WT STARD7−/−
FLAG: – – WTΔN
COXI
STARD7
ATP5α
COXI A.U. × 10⁵
N.S.
F
WT
STARD7−/−
STARD7−/− + WT
STARD7−/− + ΔN
G
Proportion (%total)
Normal cristae
Swollen cristae
H
WT STARD7−/−
FLAG: – – WTΔN
kDa
ATP5α
V2
V
I
WT
STARD7−/−
STARD7−/− + MICU1-STARD7
OCR (pmol/min/μg protein)
Measurement
J
ATP (Luminescence: RLU)
N.S.
Oligo A:
K
WT STARD7−/−
MICU1-STARD7
FLAG: – –
COXI
STARD7
ATP5α

Figure 6.

corroborate this possibility, we isolated mitochondria from *STARD7*$^{+/+}$ and *STARD7*$^{-/-}$ cells and partially solubilized mitochondrial membranes using low detergent concentrations. Proteins residing in the OM (TOMM20) or the IMS (Smac) were recovered in the supernatant, whereas IM (TIMM23) and matrix (mtHSP70)-localized proteins were present in the pellet fraction (Fig 7A). We determined the phospholipidome in both fractions by quantitative mass spectrometry (Figs 7B and EV7). In agreement with the enrichment of IM proteins, we observed increased levels of CL as well as decreased levels of PC in the pellet fraction of *STARD7*$^{+/+}$ mitochondria (Fig 7B; Vance, 2015). Strikingly, loss of STARD7 significantly impaired the accumulation of PC in the IM-enriched fraction, whereas CL and other phospholipids remained unaffected (Figs 7B and EV7). Expression of STARD7 but not of STARD7-ΔN restored PC levels in the IM fraction (Fig 7C). In light of the lipid transfer activity of recombinant STARD7 for PC (Horibata & Sugimoto, 2010; Horibata *et al*, 2016), these experiments demonstrate that STARD7 serves as an intramitochondrial LTP for PC in the IMS.

Discussion

We demonstrate that STARD7 localizes to both the cytosol and the IMS, where it functions as a LTP and shuttles PC between outer and inner mitochondrial membranes. PARL-mediated cleavage of STARD7 during its import into mitochondria and an internal sorting signal in STARD7 allow the release of a fraction of mature STARD7 into the cytosol, while another part of STARD7 remains in the mitochondrial IMS.

Several lines of evidence suggest that kinetic partitioning between STARD7 cleavage by PARL and completion of STARD7 import into mitochondria determines which fraction of STARD7 localizes to the cytosol (Fig 8). First, STARD7 completely imported into mitochondria is not released into the cytosol, demonstrating that sorting occurs during the import of newly synthesized STARD7. Second, maturation of newly imported STARD7 by another processing peptidase, the mitochondrial intermediate peptidase IMMP1L, precludes the cytosolic localization of STARD7, which accumulates quantitatively in the IMS. Previous pulse-chase experiments revealed that maturation of newly imported mitochondrial proteins by IMMP1L occurred at significantly reduced rates when compared to Smac processing by PARL (Petrungaro *et al*, 2015; Saita *et al*, 2017), suggesting that complete translocation of STARD7 across the OM prior to maturation by IMMP1L prevents its retranslocation to the cytosol. Third, depletion of TIMM23 impairs maturation of STARD7 but results in an increased release of processed STARD7 to the cytosol. Thus, membrane insertion of STARD7 by the TIM23 complex appears to facilitate PARL processing and to promote mitochondrial localization of STARD7. If membrane insertion of STARD7 is impaired upon depletion of TIMM23, PARL-mediated STARD7 cleavage results in the release of an increased fraction of mature STARD7. We therefore propose that maturation of STARD7 by PARL can occur in a TIMM23-dependent and TIMM23-independent manner and that partitioning between these pathways determines the localization of mature STARD7 to the cytosol or the IMS (Fig 8).

Further support for this model comes from the identification of negatively charged amino acid residues in the N-terminal region of mature STARD7, which serve as sorting signal for its retranslocation

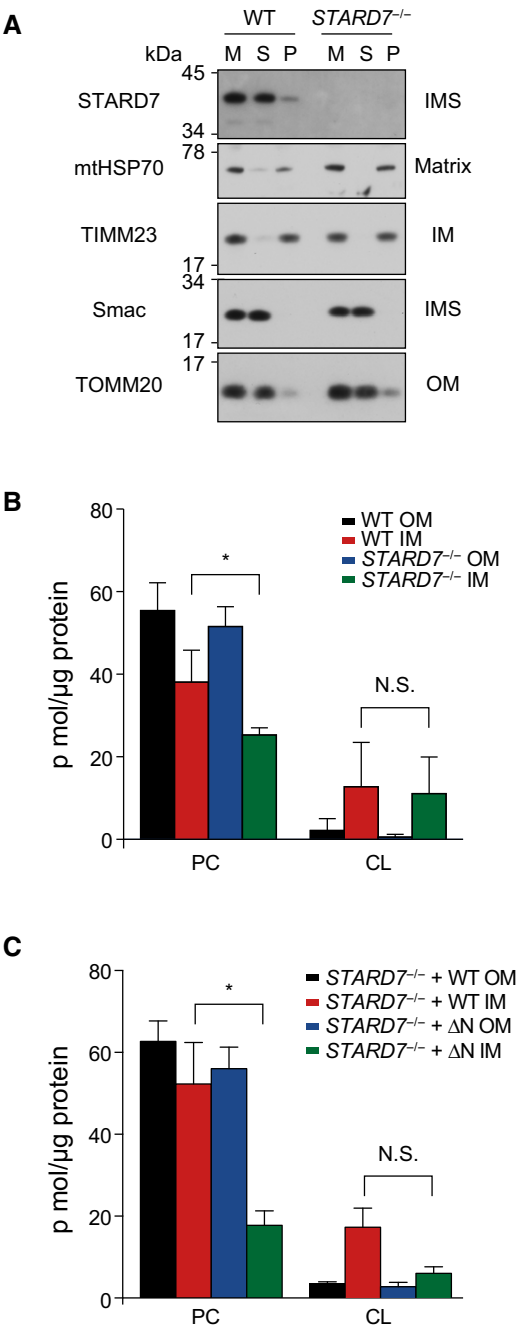

Figure 7. STARD7 is an intramitochondrial LTP for PC.

A Mitochondria (M) isolated from wild-type (WT) and *STARD7*$^{-/-}$ HeLa cells were lysed with digitonin (0.5 g digitonin/g protein for 15 min at 4°C) and split into supernatant (S; containing OM and IMS proteins) and pellet fractions (P; containing IM and matrix proteins). Samples were analyzed by SDS–PAGE and immunoblotting.

B Phospholipidome analysis of mitochondrial fractions isolated from WT and *STARD7*$^{-/-}$ HeLa cells by quantitative MS (n = 3; mean values ± SD). *$P < 0.05$, N.S., not significant, one-way ANOVA.

C Phospholipidome analysis of mitochondrial fraction isolated from *STARD7*$^{-/-}$ HeLa cells complemented with STARD7 (WT) or STARD7-ΔN by quantitative MS (n = 3; mean values ± SD). *$P < 0.05$, N.S., not significant, one-way ANOVA.

Source data are available online for this figure.

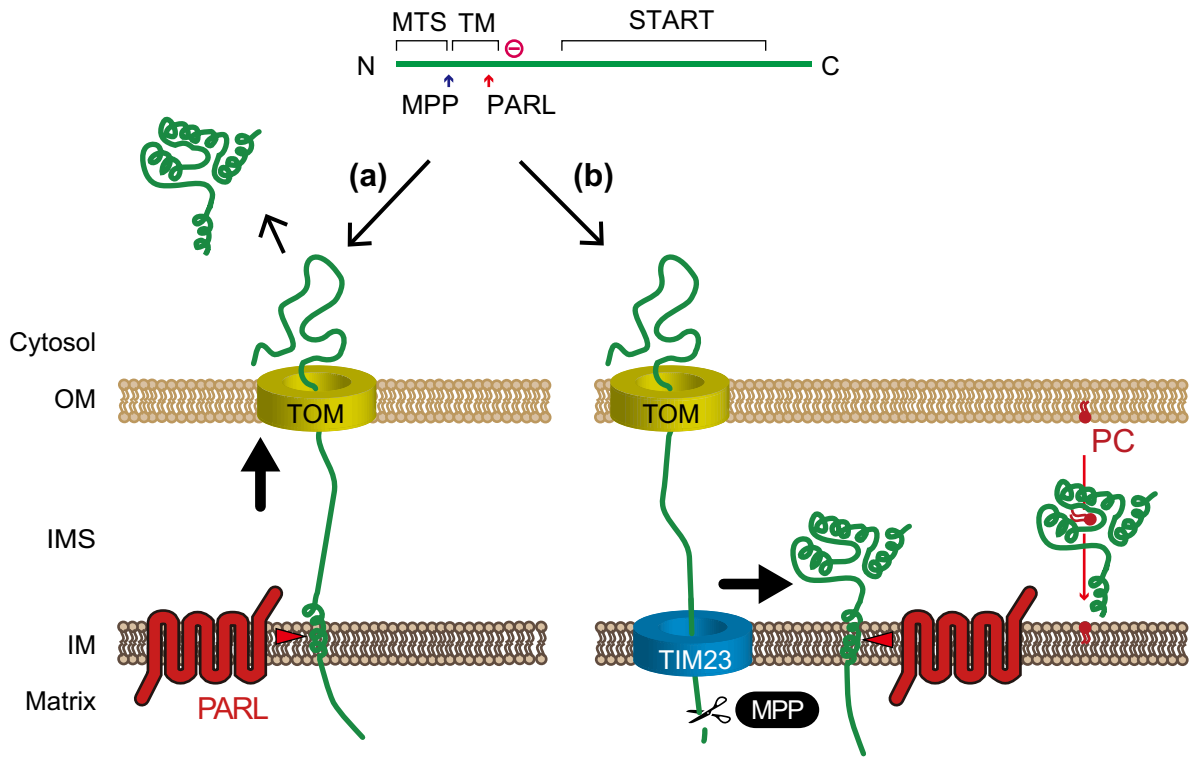

Figure 8. PARL-mediated cleavage partitions newly imported STARD7 to the cytosol and the mitochondrial intermembrane space.

Negatively charged amino acids in mature STARD7 and TIMM23 modulate sorting of newly imported STARD7 along two pathways: PARL can cleave STARD7 resulting in release of mature STARD7 into the cytosol (a). On the other hand, membrane insertion of STARD7 by the TIM23 complex delays maturation by PARL and promotes localization of mature STARD7 to the IMS, where it shuttles PC between mitochondrial membranes (b). OM, outer membrane; IMS, intermembrane space; IM, inner membrane; TOM, translocase of outer membrane; MPP, mitochondrial processing peptidase; PC, phosphatidylcholine. Arrowheads indicate PARL processing site in STARD7.

to the cytosol. Mutations in these amino acids do not affect PARL-mediated maturation but impair the cytosolic localization of STARD7. The negatively charged amino acids in STARD7 may limit binding to the TIM23 complex and thereby facilitate the release of mature STARD7 to the cytosol. Alternatively, it may modulate binding to PARL or another, yet to be identified sorting component. The STARD7-derived signal, when integrated into the corresponding region of Smac, results in the mitochondrial release of a fraction of mature Smac, which is generated by PARL during import. Thus, negatively charged amino acids following the PARL cleavage site are necessary and sufficient to allow the release of newly imported PARL substrate proteins into the cytosol.

The presence of STARD7 both in the cytosol and mitochondria substantiates the critical role of protein processing by PARL for the localization of its substrate proteins. With PINK1, the mitochondrial phosphatase PGAM5, Smac, and STARD7, four out of six known PARL substrates were found to be dually localized under various conditions. Negatively charged amino acids are present in the amino terminal regions of various PARL substrates, including the mitochondrial kinase PINK1, which is released into the cytosol upon PARL cleavage, suggesting that this signal might be of general relevance. On the other hand, the PARL substrate Smac lacks negatively charged amino acids in this region. Mature Smac accumulates quantitatively in the IMS and is only released from mitochondria in apoptotic cells in a BAX/BAK-dependent manner (Saita *et al*, 2017). We therefore propose that the partitioning of PARL substrates between the IMS and the cytosol during protein import into mitochondria depends on the presence and likely number of negatively charged amino acids in the N-terminal region of mature substrate proteins.

STARD7 has been identified as a LTP for PC in the cytosol (Horibata & Sugimoto, 2010; Horibata *et al*, 2016, 2017). Our results reveal that IMS-localized STARD7 represents a novel intramitochondrial LTP and shuttles PC between both mitochondrial membranes. Its function is related to PRELID1/TRIAP1 (Ups1/Mdm35 in yeast) and SLMO2/TRIAP1 (Ups2/Mdm35 in yeast), both members of the Ups/PRELI family of LTPs, which mediate the transport of PA and PS across the IMS, respectively (Connerth *et al*, 2012; Potting *et al*, 2013; Watanabe *et al*, 2015; Aaltonen *et al*, 2016; Miyata *et al*, 2016). Thus, LTPs mediate lipid trafficking across the IMS in a lipid-specific manner and preserve mitochondrial membrane homeostasis.

The loss of STARD7 impairs the accumulation of PC specifically in the IM but does not affect the phospholipid accumulation in the OM. Structure and function of mitochondria depend on targeting of STARD7 to mitochondria and cannot be maintained by cytosolic STARD7 or STARD7 anchored to the OM, demonstrating that mitochondrial membrane homeostasis requires STARD7-mediated PC transport across the IMS. The loss of STARD7 causes deficiencies in respiration and cristae morphogenesis. We observed an impaired dimerization of the ATP synthase in STARD7-deficient cells, which

likely contributes to the aberrant cristae formation. It is conceivable that decreased PC levels and an imbalance between PC and non-bilayer lipids such as CL and PE impair mitochondrial structure and function (Baker *et al*, 2016). Notably, PC serves as an acyl donor for CL remodeling by tafazzin (Schlame *et al*, 2012; Lu *et al*, 2016), which might explain the impaired accumulation of CL in the absence of STARD7. Thus, deficiencies in the intramitochondrial trafficking of PC have profound and pleiotropic effects on mitochondrial membrane homeostasis.

Materials and Methods

Antibodies

Rabbit polyclonal antibodies directed against PARL were described previously (Wai *et al*, 2016). The following commercially available antibodies were used: β-actin (Sigma, Cat#A5441), ATP5α (Abcam, Cat#ab14748), calnexin (Calbiochem, Cat#208880), FLAG (M2, Sigma (Cat#F1804) or Wako (Cat#018-22381)), HA (Roche, Cat#11 867423001), MICU1 (Sigma HPA037480, Cat#HPA037480), mtHSP60 (StressMarq, Cat#SMC-110), mtHSP70 (Acris, Cat#SM5084), α-MPP (Sigma, Cat#HPA021648), β-MPP (Proteintech, Cat#16064-1-AP), Myc (Cell signaling, Cat#2276), PDI (BD Biosciences, Cat#610947), SDHA (Invitrogen, Cat#459200), Smac (MBL, Cat#JM-3298-100), STARD7 (Proteintech, Cat#15689-1-AP), TIMM23 (BD Biosciences, Cat#611223), TOMM20 (Santa Cruz Biotechnology (Cat#sc-11415) or SIGMA (Cat#HPA011562)), tubulin (Sigma, Cat#T6074), YME1L (Proteintech, Cat#11510-1-AP), MFN1 (Abnova, Cat#H000556 69-M04), COXI (Molecular Probes, Cat#459600), PHB2 (BioLegend, Cat#611802), and MIC10 (Thermo Fisher Scientific, Cat# PA5-42643).

Construction of plasmids

Complementary DNA (cDNA) encoding human STARD7, Smac, and CLPB were cloned into the pcDNA3 (Invitrogen), pcDNA5/FRT/TO (Invitrogen), or pGEM4 (Addgene). For lentiviral expression, human STARD7 and IMMP1L cDNA were cloned into the pLVX-Puro (Invitrogen). Complementary DNAs encoding mutants of STARD7, TOMM70 (1–61 aa) fused to STARD7 (77–370 aa), AKAP1 (1–30 aa) fused to STARD7 (77–370 aa), and MICU1 (1–60 aa) fused to STARD7 (77–370 aa) were generated by the PCR.

Cell culture, transfection, and RNA interference

HeLa, HEK293, HEK293 Flp-In T-Rex (HEK) cells were maintained in Dulbecco's modified Eagle's medium (DMEM) supplemented with GlutaMAX (Life Technologies) and 10% fetal bovine serum and sodium pyruvate (100 μg/ml), non-essential amino acids (100 μg/ml), penicillin (100 μg/ml), and streptomycin (100 μg/ml). The cells were transfected with expression vectors using GeneJuice (Novagen) or Lipofectamine 2000 (Invitrogen), while Lipofectamine RNAiMax (Invitrogen) was used for transfection of siRNAs.

Cell viability and number were monitored using the trypan blue exclusion assay. Cells were maintained in DMEM containing 4.5 g/l glucose as described above at an initial cell number of 1×10^5. Cells were stained with 0.04% trypan blue (Life Technologies) and counted using an automated cell counter at 24-h intervals. Three replicates of the trypan blue exclusion assay were performed per data point.

CRISPR/Cas9-mediated gene editing and generation of stable cell lines

PARL$^{-/-}$ HEK293 cells were described previously (Wai *et al*, 2016). HeLa and HEK293 Flp-In T-Rex cells lacking *STARD7*, *IMMP1L*, or *YME1L* were generated using CRISPR/Cas9 gene editing. Briefly, for gene-specific DNA, fragments were synthesized, cloned into the pX335 (Addgene), and transfected into cells. After trypsinization, single cells were sorted into 96-well dishes. Surviving clones were picked, expanded, and selected based on STARD7 expression by immunoblot analysis or IMMP1L mutation by surveyor assay. Mutations were confirmed by genomic sequencing. HEK293 Flp-In T-Rex cells were transfected with pcDNA5-FRT-TO (encoding gene of interest) and pOG44 to generate stable tetracycline-inducible cell lines using GeneJuice as transfection reagent. Selection using hygromycin (100 μg/ml) was started after 2 days. For lentiviral infection, HEK293 cells were transiently transfected with pLVX-puro (containing gene of interest) for 24 h by Lenti-X™ Packaging Single Shots (VSV-G) (Takara), after which the medium was replaced with cDMEM. Then, cells were incubated for 24 h for collection of virus-containing culture supernatants. For viral infection, ~50% confluent cell cultures were exposed to virus medium with fresh cDMEM, and 4 μg/ml polybrene. Selection using puromycin (5 μg/ml) was started after 2 days.

Immunoprecipitation experiments and immunoblot analysis

Cells were lysed in RIPA buffer [50 mM HEPES/NaOH, pH 7.5, 150 mM NaCl, 1 mM EDTA, 1.0% (v/v) Triton X-100, 0.1% (w/v) SDS, 0.5% (w/v) sodium deoxycholate, protease inhibitor cocktail (Roche)] for 15 min at 4°C. After centrifugation at 16,100 *g* for 15 min at 4°C, supernatant fractions were analyzed by SDS–PAGE and immunoblotting.

For immunoprecipitation experiments, cells were lysed by incubation for 15 min at 4°C with lysis buffer [40 mM HEPES/NaOH, pH 7.5, 150 mM NaCl, 1.0% (w/v) digitonin, protease inhibitor cocktail (Roche)]. After a clarifying centrifugation at 16,100 *g* for 15 min at 4°C, supernatant fractions were subjected to immunoprecipitation and incubated for 1–2 h at 4°C with antibodies and protein G-Sepharose 4 Fast Flow (Amersham Biosciences) or EZview™ Red anti-FLAG M2 affinity gel (Sigma). After repeated washing steps, bound proteins were eluted with SDS sample buffer [50 mM Tris/HCl, pH 6.8, 2% (w/v) SDS, 5% (v/v) glycerol, 0.002% (w/v) bromophenol blue] and analyzed by SDS–PAGE and immunoblotting. Fluorescence intensities were detected using the infrared Odyssey System (Li-Cor Biosciences).

Electron microscopy

HeLa cells were incubated with 2% glutaraldehyde (in 0.12 M phosphate buffer pH 7.4, 2 h RT) for 48 h. Samples were washed with phosphate buffer and incubated 3 h in 1% osmium tetroxide (in 0.12 M phosphate buffer pH 7.4) followed by dehydration with EtOH in several steps (50, 70, 90, 100% EtOH) and embedding in

Epon (Fluka). Semithin sections were examined by light microscopy prior cutting of ultrathin sections (70 nm). Ultrathin sections were placed on 200-mesh copper grids (Electron Microscopy Sciences) and stained with uranium acetate (Plano GMBH) and lead citrate (Electron Microscopy Sciences).

Immunofluorescence staining

HeLa cells grown on glass coverslips were fixed for 10 min with 3.7% (v/v) paraformaldehyde in PBS, permeabilized by 0.2% (v/v) Triton X-100, and then incubated overnight at 4°C with primary antibodies in PBS containing 0.1% (w/v) bovine serum albumin (BSA). After washing, the cells were incubated for 1 h at RT with Alexa Fluor-labeled goat secondary antibodies at a dilution of 1:500–1:1,000 in PBS containing 0.1% (w/v) BSA. Cells were washed again and then covered with a drop of ProLong® Gold mounting reagent (P36934) (Thermo) for examination with a confocal fluorescence microscope (LSM710 META, Carl Zeiss).

Isolation of mitochondria and mitochondrial protein import

Cells were washed in PBS and resuspended in homogenization buffer (220 mM mannitol, 70 mM sucrose, 20 mM HEPES/KOH pH 7.4, 1 mM EDTA) with or without complete protease inhibitor. Cell suspension was homogenized with a rotating Teflon potter (Potter S, Braun) at 900 rpm followed by differential centrifugation. The homogenate was centrifuged at 600 *g* for 5 min at 4°C to remove the debris and nucleus, and the resulting supernatant was then centrifuged at 8,000 *g* for 15 min at 4°C to obtain mitochondrial fractions. The supernatant was centrifuged at 100,000 *g* for 30 min at 4°C to obtain cytosolic and microsomal membrane fractions. Following isolation, mitochondrial pellets (100 μg) were resuspended in 20 mM HEPES/KOH pH 7.4, 250 mM sucrose. For sodium carbonate extraction, mitochondrial pellets (100 μg) were resuspended in freshly prepared Na_2CO_3 (100 mM pH 7.4, 10.5, 11.5 or 12.5) to 0.125 mg/ml. Samples were incubated on ice for 30 min and centrifuged at 100,000 *g* for 30 min. The supernatant was subjected to TCA precipitation, and the pellet fraction was resuspended in SDS–PAGE loading buffer. For *in vitro* import of proteins into isolated mitochondria, corresponding genes were expressed *in vitro* using the TNT® Quick Coupled Transcription/Translation System (Promega). Precursor proteins were synthesized for 30 min at 30°C. Precursor proteins were incubated with mitochondria for each time points at 30°C in the absence of protease inhibitor followed by centrifugation (20,000 *g*, 5 min, 4°C). Supernatant fractions (containing released proteins) and pellet fractions (containing mitochondria) were analyzed by SDS–PAGE and immunoblotting.

For the analysis of the phospholipidome, mitochondria were further purified by density gradient centrifugation: mitochondria were layered on top of a Percoll step gradient [12, 19, 40% Percoll in isolation buffer IB (5 mM HEPES/KOH pH 7.4, 220 mM mannitol, 70 mM sucrose and 1 mM EGTA pH 8.0)] followed by ultracentrifugation (42,000 *g*, 30 min, 4°C) in SW41Ti rotor (Beckman). The mitochondrial fraction was isolated and diluted 1:5 in IB and washed three times by IB (16,100 *g*, 5 min, 4°C). For isolation of OM and IM, mitochondria (200 μg) were suspended in 10 μl buffer H (2 mM HEPES/KOH pH 7.4, 220 mM mannitol, 70 mM sucrose, and complete protease inhibitor) with 0.5 mg/ml BSA, and incubated with 10 μl of 10 mg/ml digitonin containing buffer H for 15 min at 4°C. The reaction is terminated by buffer H with 5 mg/ml BSA and centrifuged at 12,000 *g* for 15 min to obtain OM fractions as supernatant, and the resulting pellet was washed with 100 μl buffer H with 0.5 mg/ml BSA and centrifuged at 12,000 *g* for 15 min to obtain IM fractions as pellet.

Subfractionation of mitochondria

Mitochondria were treated with 0.5 μg/ml proteinase K (PK) for 10 min with or without osmotic swelling in 10 mM HEPES-KOH pH 7.4 containing 1 mM EDTA. PK digestion of mitochondrial proteins was stopped with 1 mM PMSF. When indicated, 0.5% (v/v) Triton X-100 was added prior to PK treatment. Samples were precipitated by trichloric acid and analyzed by SDS–PAGE and immunoblotting.

Quantitative mass spectrometry of phospholipids

Mass spectrometric analysis was performed essentially as described (Tatsuta, 2017). Lipids were extracted from isolated pure mitochondria, digitonin-treated membrane fractions, or whole cells in the presence of internal standards of major phospholipids (PC 17:0–20:4, PE 17:0–20:4, PI 17:0–20:4, PS 17:0–20:4, PG 17:0–20:4, PA 17:0–20:4, all from Avanti Polar Lipids) and CL (CL mix I, Avanti Polar Lipids). Extraction was performed according to Bligh and Dyer with modifications. Briefly, 10 μg mitochondria or 0.25 million cells in 0.24 ml water and internal standards (100, 60, 35, 25, 15, 15, and 24 pmole of PC 17:0–20:4, PE 17:0–20:4, PI 17:0–20:4, PS 17:0–20:4, PG 17:0–20:4, PA 17:0–20:4, and CLs, respectively) were mixed with 0.9 ml of chloroform/methanol [40:80 (v/v)] for 10 min. After addition of 0.3 ml chloroform and of 0.3 ml H_2O, the sample was mixed again for 10 min, and phase separation was induced by centrifugation (800 *g*, 2 min). The lower chloroform phase was carefully transferred to a clean glass vial. The upper water phase was mixed with 10 μl 1N HCl and 300 μl chloroform for 10 min. After phase separation, the lower chloroform phase was carefully transferred to the glass vial with the chloroform phase from the first extraction. The solvent was evaporated by a gentle stream of argon at 37°C. Lipids were dissolved in 10 mM ammonium acetate in methanol, transferred to Twin.tec PCR plate sealed with Thermowell sealing tape, and analyzed on a QTRAP 6500 triple quadrupole mass spectrometer (SCIEX) equipped with nano-infusion splay device (TriVersa NanoMate with ESI-Chip type A, Advion).

Analysis of mitochondrial function

Oxygen consumption rates (OCR) were measured with a Seahorse Extracellular Flux Analyzer XF24 (Seahorse Bioscience). HeLa cells were plated into each well one day before the assay. The OCR was normalized for the total amount of protein. Data are presented as the means ± standard error of the mean (SEM) of four to nine replicates. For the determination of the cellular ATP content, HeLa cells were plated and grown overnight in 25 mM glucose medium, and grown for another day in 10 mM galactose medium. Cells were incubated with or without 50 nM oligomycin A for 4 h. Whole-cell ATP content was measured by CellTiter-Glo Luminescent Cell Viability/ATP Assay kit (Promega).

Blue native-PAGE analysis

Blue native-PAGE was performed as described previously with some modifications (Wittig *et al*, 2006). In brief, mitochondria (100 μg) were lysed in solubilization buffer [50 mM NaCl, 5 mM 6-amino-hexanoic acid, 50 mM imidazole/HCl (pH 7.0), 10% (v/v) glycerol, 50 mM KPi-buffer (pH 7.4)] containing 1 or 6 g digitonin/g protein. Lysates were centrifuged, supplemented with 0.1% (w/v) CBB, and separated by 3%–13% BN-PAGE.

Liposome preparation and reconstitution of PARL

For liposome preparation, a phospholipid composition similar to IM was chosen as described (Schwarz *et al*, 2007). Lipids (10 mM dioleoyl phosphatidylcholine, 8.45 mM dioleoyl phosphatidylethanolamine, 4.5 mM cardiolipin, 0.75 mM dioleoyl phosphatidylserine, 1.25 mM phosphatidylinositol isolated from soybeans, and 0.01 mM rhodamine phosphatidylethanolamine) were mixed together, and chloroform was evaporated under argon flow at 37°C. Liposomes were dissolved in buffer LP (5 mM Tris/HCl pH 8.5, 10 mM KOAc) by vortexing, and a liposome extrusion was performed with a mini extruder according to the manufacturer's protocol (Avanti polar lipids) by use of two supporter membranes and a polycarbonate membrane (Avanti polar lipids, 0.1 μM). Mature, human PARL harboring a hexahistidine-tag at its C-terminus was expressed in a bacterial lysate-based, continuous-exchange cell-free expression system using pIVEX2.3d-PARL^{His} (amino acids F54–K380) or pIVEX2.3d-PARL(S277A)^{His} vector in the presence of liposomes. Maximal protein expression was achieved by shaking at 30°C for 16 h with 16 mM $Mg(OAc)_2$ and 270 mM KOAc. Liposomes with incorporated PARL proteins were harvested by centrifugation (20 min, 16,000 *g*, 4°C) and washed twice with buffer FB (5 mM HEPES/KOH pH 7.4, 25 mM NaCl). Soluble and insoluble proteoliposomes were overlayed by a 40, 30, 15, and 0% sucrose step gradient and separated by centrifugation (200,000 *g*, 2 h, 4°C) in buffer FB. The top fraction with soluble PARL proteoliposomes harbors the active protein.

Statistical analyses

Quantitative data are presented as means ± SD if not indicated otherwise. The statistical significance was assessed using one-way ANOVA. A *P*-value of < 0.05 was considered statistically significant.

Expanded View for this article is available online.

Acknowledgements

We thank Janine Klask for excellent technical support, Dr. Thomas MacVicar for *YME1L*$^{-/-}$ cells, Dr. Astrid Schauss (CECAD imaging facility) for support in electron microscopy, and Dr. Jan Riemer for fruitful discussions. This work was supported by a fellowship of the Japan Society for the Promotion of Science (JSPS) for research abroad to S.S. and Y.O. and a Reinhart-Koselleck-grant of the Deutsche Forschungsgemeinschaft (DFG) to T.L.

Author contributions

SS and TL designed the research. TT determined the phospholipidome by mass spectrometry, PAL reconstituted PARL, and TK, together with SS, performed mitochondrial import experiments. YO and SS established the fractionation of mitochondria. SS performed all other experiments. SS and TL wrote the manuscript with the comments of the other authors.

Conflict of interest

The authors declare that they have no conflict of interest.

References

Aaltonen MJ, Friedman JR, Osman C, Salin B, di Rago JP, Nunnari J, Langer T, Tatsuta T (2016) MICOS and phospholipid transfer by Ups2-Mdm35 organize membrane lipid synthesis in mitochondria. *J Cell Biol* 213: 525 – 534

Alpy F, Tomasetto C (2014) START ships lipids across interorganelle space. *Biochimie* 96: 85 – 95

Baker CD, Basu Ball W, Pryce EN, Gohil VM (2016) Specific requirements of nonbilayer phospholipids in mitochondrial respiratory chain function and formation. *Mol Biol Cell* 27: 2161 – 2171

Bottani E, Cerutti R, Harbour ME, Ravaglia S, Dogan SA, Giordano C, Fearnley IM, D'Amati G, Viscomi C, Fernandez-Vizarra E, Zeviani M (2017) TTC19 plays a husbandry role on UQCRFS1 turnover in the biogenesis of mitochondrial respiratory complex III. *Mol Cell* 67: 96 – 105

Capo-Chichi JM, Boissel S, Brustein E, Pickles S, Fallet-Bianco C, Nassif C, Patry L, Dobrzeniecka S, Liao M, Labuda D, Samuels ME, Hamdan FF, Vande Velde C, Rouleau GA, Drapeau P, Michaud JL (2015) Disruption of CLPB is associated with congenital microcephaly, severe encephalopathy and 3-methylglutaconic aciduria. *J Med Genet* 52: 303 – 311

Chen G, Han Z, Feng D, Chen Y, Chen L, Wu H, Huang L, Zhou C, Cai X, Fu C, Duan L, Wang X, Liu L, Liu X, Shen Y, Zhu Y, Chen Q (2014) A regulatory signaling loop comprising the PGAM5 phosphatase and CK2 controls receptor-mediated mitophagy. *Mol Cell* 54: 362 – 377

Cipolat S, Rudka T, Hartmann D, Costa V, Serneels L, Craessaerts K, Metzger K, Frezza C, Annaert W, D'Adamio L, Derks C, Dejaegere T, Pellegrini L, D'Hooge R, Scorrano L, De Strooper B (2006) Mitochondrial rhomboid PARL regulates cytochrome c release during apoptosis via OPA1-dependent cristae remodeling. *Cell* 126: 163 – 175

Civitarese AE, MacLean PS, Carling S, Kerr-Bayles L, McMillan RP, Pierce A, Becker TC, Moro C, Finlayson J, Lefort N, Newgard CB, Mandarino L, Cefalu W, Walder K, Collier GR, Hulver MW, Smith SR, Ravussin E (2010) Regulation of skeletal muscle oxidative capacity and insulin signaling by the mitochondrial rhomboid protease PARL. *Cell Metab* 11: 412 – 426

Connerth M, Tatsuta T, Haag M, Klecker T, Westermann B, Langer T (2012) Intramitochondrial transport of phosphatidic acid in yeast by a lipid transfer protein. *Science* 338: 815 – 818

Dusterhoft S, Kunzel U, Freeman M (2017) Rhomboid proteases in human disease: mechanisms and future prospects. *Biochim Biophys Acta* 1864: 2200 – 2209

Frezza C, Cipolat S, Martins de Brito O, Micaroni M, Beznoussenko GV, Rudka T, Bartoli D, Polishuck RS, Danial NN, De Strooper B, Scorrano L (2006) OPA1 controls apoptotic cristae remodeling independently from mitochondrial fusion. *Cell* 126: 177 – 189

Ghezzi D, Arzuffi P, Zordan M, Da Re C, Lamperti C, Benna C, D'Adamo P, Diodato D, Costa R, Mariotti C, Uziel G, Smiderle C, Zeviani M (2011) Mutations in TTC19 cause mitochondrial complex III deficiency and neurological impairment in humans and flies. *Nat Genet* 43: 259 – 263

Habersetzer J, Larrieu I, Priault M, Salin B, Rossignol R, Brethes D, Paumard P (2013) Human F1F0 ATP synthase, mitochondrial ultrastructure and OXPHOS impairment: a (super-)complex matter? *PLoS One* 8: e75429

Horibata Y, Sugimoto H (2010) StarD7 mediates the intracellular trafficking of phosphatidylcholine to mitochondria. *J Biol Chem* 285: 7358 – 7365

Horibata Y, Ando H, Zhang P, Vergnes L, Aoyama C, Itoh M, Reue K, Sugimoto H (2016) StarD7 protein deficiency adversely affects the phosphatidylcholine composition, respiratory activity, and cristae structure of mitochondria. *J Biol Chem* 291: 24880 – 24891

Horibata Y, Ando H, Satou M, Shimizu H, Mitsuhashi S, Shimizu Y, Itoh M, Sugimoto H (2017) Identification of the N-terminal transmembrane domain of StarD7 and its importance for mitochondrial outer membrane localization and phosphatidylcholine transfer. *Sci Rep* 7: 8793

Jin SM, Lazarou M, Wang C, Kane LA, Narendra DP, Youle RJ (2010) Mitochondrial membrane potential regulates PINK1 import and proteolytic destabilization by PARL. *J Cell Biol* 191: 933 – 942

Kanabus M, Shahni R, Saldanha JW, Murphy E, Plagnol V, Hoff WV, Heales S, Rahman S (2015) Bi-allelic CLPB mutations cause cataract, renal cysts, nephrocalcinosis and 3-methylglutaconic aciduria, a novel disorder of mitochondrial protein disaggregation. *J Inherit Metab Dis* 38: 211 – 219

Lu YW, Galbraith L, Herndon JD, Lu YL, Pras-Raves M, Vervaart M, Van Kampen A, Luyf A, Koehler CM, McCaffery JM, Gottlieb E, Vaz FM, Claypool SM (2016) Defining functional classes of Barth syndrome mutation in humans. *Hum Mol Genet* 25: 1754 – 1770

McLelland GL, Soubannier V, Chen CX, McBride HM, Fon EA (2014) Parkin and PINK1 function in a vesicular trafficking pathway regulating mitochondrial quality control. *EMBO J* 33: 282 – 295

Miyata N, Watanabe Y, Tamura Y, Endo T, Kuge O (2016) Phosphatidylserine transport by Ups2-Mdm35 in respiration-active mitochondria. *J Cell Biol* 214: 77 – 88

Morais VA, Haddad D, Craessaerts K, De Bock PJ, Swerts J, Vilain S, Aerts L, Overbergh L, Grunewald A, Seibler P, Klein C, Gevaert K, Verstreken P, De Strooper B (2014) PINK1 loss-of-function mutations affect mitochondrial complex I activity via NdufA10 ubiquinone uncoupling. *Science* 344: 203 – 207

Narendra DP, Jin SM, Tanaka A, Suen DF, Gautier CA, Shen J, Cookson MR, Youle RJ (2010) PINK1 is selectively stabilized on impaired mitochondria to activate Parkin. *PLoS Biol* 8: e1000298

Panda S, Srivastava S, Li Z, Vaeth M, Fuhs SR, Hunter T, Skolnik EY (2016) Identification of PGAM5 as a mammalian protein histidine phosphatase that plays a central role to negatively regulate CD4(+) T cells. *Mol Cell* 63: 457 – 469

Paumard P, Vaillier J, Coulary B, Schaeffer J, Soubannier V, Mueller DM, Brethes D, di Rago JP, Velours J (2002) The ATP synthase is involved in generating mitochondrial cristae morphology. *EMBO J* 21: 221 – 230

Perocchi F, Gohil VM, Girgis HS, Bao XR, McCombs JE, Palmer AE, Mootha VK (2010) MICU1 encodes a mitochondrial EF hand protein required for Ca (2+) uptake. *Nature* 467: 291 – 296

Petrungaro C, Zimmermann KM, Kuttner V, Fischer M, Dengjel J, Bogeski I, Riemer J (2015) The Ca(2+)-dependent release of the Mia40-induced MICU1-MICU2 dimer from MCU regulates mitochondrial Ca(2+) uptake. *Cell Metab* 22: 721 – 733

Potting C, Tatsuta T, Konig T, Haag M, Wai T, Aaltonen MJ, Langer T (2013) TRIAP1/PRELI complexes prevent apoptosis by mediating intramitochondrial transport of phosphatidic acid. *Cell Metab* 18: 287 – 295

Quiros PM, Langer T, Lopez-Otin C (2015) New roles for mitochondrial proteases in health, ageing and disease. *Nat Rev Mol Cell Biol* 16: 345 – 359

Rampelt H, Zerbes RM, van der Laan M, Pfanner N (2017) Role of the mitochondrial contact site and cristae organizing system in membrane architecture and dynamics. *Biochim Biophys Acta* 1864: 737 – 746

Rauschenberger V, Bernkopf DB, Krenn S, Jalal K, Heller J, Behrens J, Gentzel M, Schambony A (2017) The phosphatase Pgam5 antagonizes Wnt/beta-Catenin signaling in embryonic anterior-posterior axis patterning. *Development* 144: 2234 – 2247

Saita S, Nolte H, Fiedler KU, Kashkar H, Venne AS, Zahedi RP, Krüger M, Langer T (2017) PARL mediates Smac proteolytic maturation in mitochondria to promote apoptosis. *Nat Cell Biol* 19: 318 – 328

Saunders C, Smith L, Wibrand F, Ravn K, Bross P, Thiffault I, Christensen M, Atherton A, Farrow E, Miller N, Kingsmore SF, Ostergaard E (2015) CLPB variants associated with autosomal-recessive mitochondrial disorder with cataract, neutropenia, epilepsy, and methylglutaconic aciduria. *Am J Hum Genet* 96: 258 – 265

Schlame M, Acehan D, Berno B, Xu Y, Valvo S, Ren M, Stokes DL, Epand RM (2012) The physical state of lipid substrates provides transacylation specificity for tafazzin. *Nat Chem Biol* 8: 862 – 869

Schwarz D, Junge F, Durst F, Frolich N, Schneider B, Reckel S, Sobhanifar S, Dotsch V, Bernhard F (2007) Preparative scale expression of membrane proteins in Escherichia coli-based continuous exchange cell-free systems. *Nat Protoc* 2: 2945 – 2957

Sekine S, Kanamaru Y, Koike M, Nishihara A, Okada M, Kinoshita H, Kamiyama M, Maruyama J, Uchiyama Y, Ishihara N, Takeda K, Ichijo H (2012) Rhomboid protease PARL mediates the mitochondrial membrane potential loss-induced cleavage of PGAM5. *J Biol Chem* 287: 34635 – 34645

Spinazzi M, De Strooper B (2016) PARL: the mitochondrial rhomboid protease. *Semin Cell Dev Biol* 60: 19 – 28

Takeda K, Komuro Y, Hayakawa T, Oguchi H, Ishida Y, Murakami S, Noguchi T, Kinoshita H, Sekine Y, Iemura S, Natsume T, Ichijo H (2009) Mitochondrial phosphoglycerate mutase 5 uses alternate catalytic activity as a protein serine/threonine phosphatase to activate ASK1. *Proc Natl Acad Sci USA* 106: 12301 – 12305

Tatsuta T (2017) Quantitative analysis of glycerophospholipids in mitochondria by mass spectrometry. *Methods Mol Biol* 67: 79 – 103

Tatsuta T, Langer T (2017) Prohibitins. *Curr Biol* 27: R629 – R631

Urban S (2016) A guide to the rhomboid protein superfamily in development and disease. *Semin Cell Dev Biol* 60: 1 – 4

Vance JE (2015) Phospholipid synthesis and transport in mammalian cells. *Traffic* 16: 1 – 18

Wai T, Saita S, Nolte H, Muller S, Konig T, Richter-Dennerlein R, Sprenger HG, Madrenas J, Muhlmeister M, Brandt U, Kruger M, Langer T (2016) The membrane scaffold SLP2 anchors a proteolytic hub in mitochondria containing PARL and the i-AAA protease YME1L. *EMBO Rep* 17: 1844 – 1856

Wang Z, Jiang H, Chen S, Du F, Wang X (2012) The mitochondrial phosphatase PGAM5 functions at the convergence point of multiple necrotic death pathways. *Cell* 148: 228 – 243

Watanabe Y, Tamura Y, Kawano S, Endo T (2015) Structural and mechanistic insights into phospholipid transfer by Ups1-Mdm35 in mitochondria. *Nat Commun* 6: 7922 – 7934

Whitworth AJ, Pallanck LJ (2017) PINK1/Parkin mitophagy and neurodegeneration-what do we really know *in vivo*? *Curr Opin Genet Dev* 44: 47 – 53

Wiedemann N, Pfanner N (2017) Mitochondrial machineries for protein import and assembly. *Annu Rev Biochem* 86: 685 – 714

Wittig I, Carrozzo R, Santorelli FM, Schagger H (2006) Supercomplexes and subcomplexes of mitochondrial oxidative phosphorylation. *Biochem Biophys Acta* 1757: 1066 – 1072

Wortmann SB, Zietkiewicz S, Kousi M, Szklarczyk R, Haack TB, Gersting SW, Muntau AC, Rakovic A, Renkema GH, Rodenburg RJ, Strom TM, Meitinger T, Rubio-Gozalbo ME, Chrusciel E, Distelmaier F, Golzio C, Jansen JH, van

Karnebeek C, Lillquist Y, Lucke T *et al* (2015) CLPB mutations cause 3-methylglutaconic aciduria, progressive brain atrophy, intellectual disability, congenital neutropenia, cataracts, movement disorder. *Am J Hum Genet* 96: 245 – 257

Yamano K, Youle RJ (2013) PINK1 is degraded through the N-end rule pathway. *Autophagy* 9: 1758 – 1769

Yang L, Lewkowich I, Apsley K, Fritz JM, Wills-Karp M, Weaver TE (2015) Haploinsufficiency for Stard7 is associated with enhanced allergic responses in lung and skin. *J Immunol* 194: 5635 – 5643

Yang L, Na CL, Luo S, Wu D, Hogan S, Huang T, Weaver TE (2017) The phosphatidylcholine transfer protein Stard7 is required for mitochondrial and epithelial cell homeostasis. *Sci Rep* 7: 46416

